Effect of seatbelt and airbag loads on thoracic injury risk in frontal crashes considering average and small body sizes and age-dependent thoracic fragility

Jacobo Antona-Makoshi, Yoshihiro Yamamoto, Ryosuke Kato, Shouhei Kunitomi, Atsuhiro Konosu, Yasuhiro Dokko, Tsuyoshi Yasuki, Tomoaki Takamiya

Abstract This study evaluates the effect of age-dependent thoracic fragility and reduced body size on thoracic injury risk in full frontal crashes under a wide range of seatbelt and airbag settings. A total of 36 full frontal 56 km/h crash simulations were conducted with three JAMA human body models (Adult AM50, Elderly AM50 and Elderly Small) and a vehicle interior model. The human models were positioned on the driver's seat and were restrained with a conventional three point seatbelt. Three levels of airbag load and four levels of belt force limit were combined. Simulations with the Adult AM50 model predicted no rib fracture under the wide range of restraints settings. The models with thoracic properties representative of Elderly predicted large numbers of rib fractures for belt force limits of 4 kN or higher, regardless of body size and airbag settings. Reduced belt force limits led to a lower number of predicted rib fractures. However, this reduction was achieved at the cost of increased body forward excursion. This led to head strikethrough events in some cases with the AM50 models. The results highlight the importance of accounting for age-dependent thoracic fragility and body size in search of optimal thoracic protection for diverse populations, including the elderly.

Keywords Thoracic Injuries, Frontal Crashes, Ageing, Human Finite Element Models

I. INTRODUCTION

Thoracic injuries comprise a large amount of the injuries sustained by occupants involved in frontal crashes [1-3]. The risks of fatal and severe injuries are higher for older than for younger occupants [1][4] due to increased fragility of the thorax with age [5]. In addition, the restraints systems may not be optimal for all occupants ages and anthropometries [6]. These issues are of particular concern in Japan, where the proportion of elderly is the largest [7] and the population stature is smaller than in Europe and in the US [8]. In Japan, the elderly account for more than half of the traffic related fatalities and severe injuries [3], with male elderly drivers exposed to the highest risk of sustaining a thorax injury [2]. According to projected societal trends [7] , the current situation will increase in significance not only in Japan but also in most of the developed countries in the following decades.

The introduction of seatbelts and air bags has significantly contributed to the decline in number of fatalities and severe injuries in frontal crashes [9]. The fatality risk for occupants wearing a seatbelt in a vehicle fitted with air bags in frontal crashes is reduced by 61 percent compared to occupants not wearing such restraints [10]. Despite their effectiveness, a large amount of fatal thoracic injuries still occur in frontal crashes involving occupants wearing seatbelts and air bag deployment [11]. This provides an opportunity to continue improving occupant thoracic protection through the refinement of restraint systems.

A straightforward solution to mitigate thoracic injury risk could be reducing the severity of thoracic loads by decreasing the belt force limit. However, the potential disadvantages of simply adjusting belt load without anticipating the full excursion of a human occupant have been highlighted in previous studies with 50th percentile male (AM50) and 5th percentile female (AF05) Hybrid III (HIII) dummies [6], in frontal crash tests with AM50 HIII and THOR dummies [12] and in simulated frontal crashes with human body finite element (FE) models of different sizes (AF05, AM50, AM95) [13]. As new restraint system configurations are developed, comprehensive research strategies that enable optimal protection also for populations which anthropometry is

J. Antona-Makoshi (tel: +81-29-856-0885, e-mail: ajacobo@jari.or.jp), Y. Yamamoto, R. Kato, S. Kunitomi and A. Konosu are research engineers at the Japan Automobile Research Institute (JARI) in Tsukuba, Japan. Y. Dokko, T. Yasuki, and T. Takamiya are members of the Japan Automobile Manufacturers Association, Inc. (JAMA) in Tokyo, Japan.

not covered by the dummies and that also account for the fragility of the elderly must be deployed.

Human body finite element (FE) models, used as complementary tools to crash test dummies, enable assessments of restraint performance early in the design of new restraint systems. These models have the potential to predict injuries in greater detail compared to dummies [14]. In addition, human FE models can easily be designed to account for population factors such as body size or age-specific characteristics. Human FE models of different sizes (AF05, AM50, AM95) have been applied to investigate the effect of body size on thoracic injury risks under a large range of combined belt force limits and air bag settings [13]. The past studies did however not account for the possible effect that age has in thoracic injury risk. Currently, several human FE models that account for thoracic ageing properties are available [15-18]. Within these models, the one developed by the Japan Automobile Manufacturers Association (JAMA) has been specifically designed to account for age-dependent thoracic characteristics and the reduced size of Japanese elderly [18].

The ultimate goal of this research is to contribute to the reduction of vehicle occupant thoracic injuries due to traffic crashes, especially in elderly. The specific aim is to evaluate, by means of a parametric study with human FE models, the effect of age-dependent thoracic fragility and reduced body size on thoracic injury risk in full frontal crashes under a wide range of seatbelt and airbag settings.

II. METHODS

A human body FE model previously developed and validated by the JAMA [18] and a mid-sedan vehicle interior sled-type model developed by the Japan Automobile Research Institute (JARI) were utilised in this study. The human model accounts for two body size settings, one representative of an AM50 (175 cm and 77 kg) and one representative of an average size Japanese elderly male, thereafter denoted as *Small* (161 cm and 60 kg). In addition, thoracic properties of the model can be adapted to different ages from 20 to 75 years of age. In the current study, the two body size settings (AM50 and *Small*) were combined with two thoracic age settings (Adult of 45 and Elderly 75 years of age) to generate three occupant models (TABLE I).

TABLE I Occupant models names, body size and age settings used in this study

Model Name	Height (cm)	Weight (kg)	Age settings (years)
Adult AM50	175	77	45
Elderly AM50	175	77	75
Elderly *Small*	161	60	75

The JARI vehicle interior model includes a non-deformable vehicle frame, a mass production seat, a collapsible steering column with airbag, instrument panel, knee bolster, floor pan and pedals. The overall layout of these elements was defined according to data from a mid-size sedan vehicle. Seat and seatbelt layouts were further adjusted to driver's height according to data from a survey on preferred driving positions, conducted by the JAMA (described below). The driver models were restrained with a conventional three point seatbelt with a pre-tensioner and a variable force limiter. A 56 km/h full frontal equivalent impact barrier pulse was defined based on a real car crash test. Under these conditions, a total of 36 crash simulations were conducted by combining the three driver models (Adult AM50, Elderly AM50 and Elderly *Small*) with three airbag pressure settings (denoted as Low, Mid, and High) and four levels of belt force limit (2, 3, 4 and 5 kN). Full body kinematics, belt and airbag loads, chest deflection, and predicted location and number of ribs fractured were collected from the simulations and analysed case-by-case. All simulations were run with LS-Dyna (mpp971s R7.1.1). Figure 1 summarises the crash simulation model including drivers, vehicle, restraints systems models, and data sources used in this study. Detailed descriptions of these models and data are provided below.

Driver FE Models and age-dependent thoracic properties

The human FE model was developed and validated in several stages. A brief summary of the model development, validation process and results, and model availability is presented in Appendix A. More detailed descriptions can be found in [18]. In short, a detailed thoracic model was developed from medical images of a small (161 cm and 60 kg) elderly Post Mortem Human Subject (PMHS). Validation was conducted at both

component and assembled level against large amount of experimental data obtained from the elderly PMHS. Age-dependent thoracic properties were assigned to different thoracic components according to the literature. These properties included rib cortical bone thickness [19][20], material properties [20][[21], and ultimate strain [22], as well as costal cartilage material properties [23] and muscle/flesh material properties in tension and compression [23][24]. Thereafter, the thoracic model was complemented with the head and the extremities of a previously developed model and linearly scaled up to AM50 size. The AM50 size model with thoracic settings representative of an Adult (45 years) and an Elderly (75 years) person was validated against existing full scale biomechanical data from the literature. The validation data included age-dependent corridors developed from hub-to-thorax impact tests with PMHS [17][25] and frontal impact sled PMHS test data [26]. The age-dependent thoracic properties utilised to validate the model and also in the current simulation study are presented in Figure 2. The results from the model validation model using these properties are summarised in Figure A1 (Appendix A). Overall, the model presented sensitivity to both size and age dependent characteristics in hub and frontal sled tests conditions. In frontal impact sled conditions, the model showed good 3-dimensional head and spine kinematics, as well as rib cage multipoint deflections. When properties representative of an aging person were simulated, both the rib cage deformation and the predicted number of rib fractures increased, following similar trends to the corresponding sets of experiments.

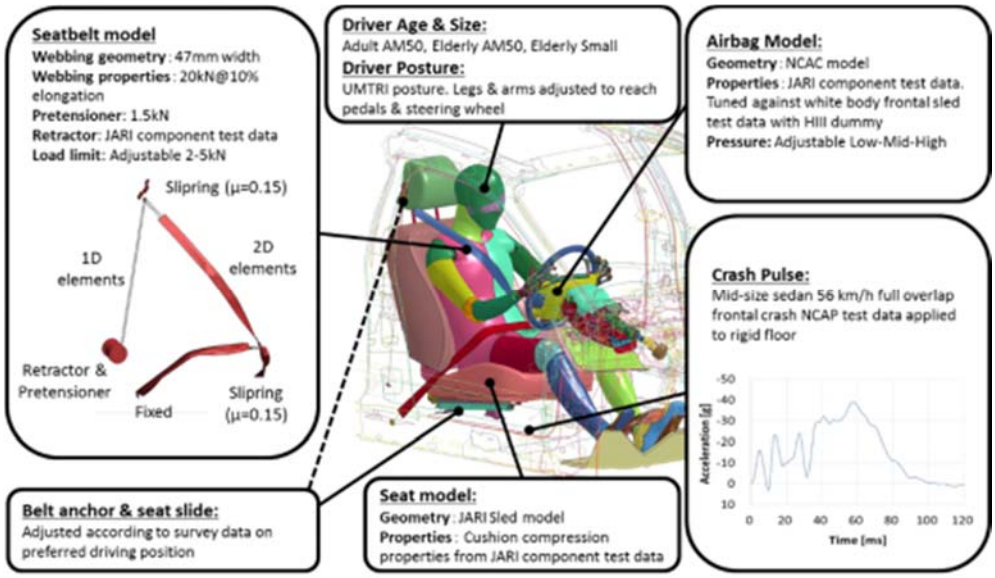

Figure 1 Summary of driver, vehicle and restraints models, and data sources used in this study

Vehicle FE Model

The JARI vehicle interior FE model is a cabin-type sled model which was initially developed from a mid-size sedan vehicle. For this study, the overall layout of the different vehicle components was defined according to the data presented in Figure B2 (Appendix B). These data were measured by hand directly from a real vehicle. Preliminary mechanical properties for different components such as the seat cushion, seatbelt, airbag and knee bolster were implemented based on past component test data conducted at the JARI. These properties were reviewed, modified when required, and approved for this study as acceptable average properties for a mid-size sedan type vehicle. Thereafter, an evaluation of the overall behavior of the vehicle model and restraints was conducted by simulating an impact deceleration equivalent to a 55 km/h frontal crash against a rigid wall. This simulation was conducted with a restrained HIII dummy FE model (LSTC, Livermore, USA). The results from this simulation were compared to a white-body frontal sled test conducted with a HIII dummy under the same deceleration conditions and with a similar restraint systems environment [27]. Images of the JARI vehicle model, of the white-body sled and a comparison of the results from the simulation and the test are shown in Figure C4 (Appendix C). This evaluation confirmed that the vehicle model had an acceptable behavior in terms of restraint loads and dummy readings in a full frontal crash. Hence, the vehicle FE model was considered appropriate for this study.

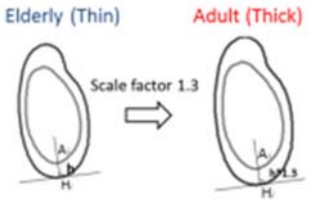

a) Rib Cortical bone thickness

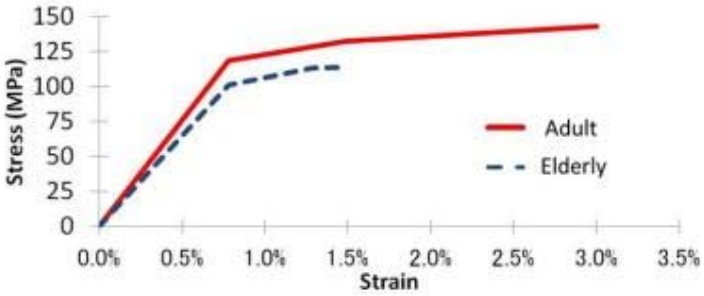

b) Rib Cortical bone material properties and failure strain

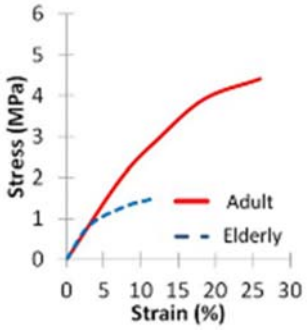

c) Costal cartilage material properties

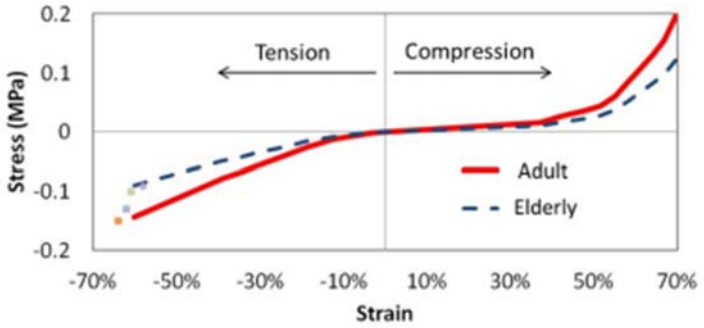

d) Flesh material properties

Figure 2. Thoracic age dependent settings used in this study

Seatbelt and Airbag Models

A conventional three point seatbelt model with two slip rings and a simple pyro-technique retractor with a pre-tensioner was developed (Figure 1). The belt webbing model combined 2D membrane elements in the parts likely to contact the occupant with 1D seatbelt elements in the parts likely to pass through the slip rings. Tensile properties of the belt webbing were set to 20 kN at 10% elongation. Friction coefficient between the 1D belt elements and the slip rings was set to 0.15. The retractor pre-tensioner was set to trigger at 17 ms from the initiation of the crash and produced a belt force of approximately 1.5 kN within 5 ms from trigger. Locked retractor properties were defined by a belt force-belt payout distance curve with a slope of approximately 150 N/mm. Four different belt force limits were defined by tuning this curve to different plateau force levels so they produced 2, 3, 4, or 5 kN belt force at a 1D seatbelt element located nearby the shoulder of the driver model.

A simple airbag model was developed by combining the geometry of an open source (60 litre) airbag model with airbag properties from the JARI component database. The original model from which the geometry was obtained was developed by The National Crash Analysis Center (NCAC) of The George Washington University under a contract with the National Highway Traffic Safety Administration (NHTSA). The case of the airbag was connected to the collapsible column in the JARI vehicle model and was tuned according to the JARI data. The airbag was set to trigger at 20 ms from the beginning of the crash. An input mass flow rate curve with a peak of approximately 2 kg/s at 10 ms from trigger was implemented. Three different airbag pressure settings (Low, Mid and High) were defined by modifying the size of the ventilation hole in the model according to input from experts. Such adjustments produced airbag to thorax contact load changes in the order of 1 to 2 kN, depending on occupant body size and forward traveling distance.

Seat position and Seatbelt Anchorages Layout

Seat position and seatbelt anchorages layout was set according to a sub-set of data on preferred driving position obtained from a survey conducted by the JAMA. The sub-set included 99 male and female adult volunteers and a mid-size sedan vehicle. Age, height and weight of the volunteers were collected. The seat slide (horizontal) position, seat (vertical) lift, seatback inclination and shoulder belt anchor were initially set to neutral positions. Thereafter, the participants were asked to get on the car and adjust these parameters for comfortable driving posture. For the purpose of the current simulation study, the survey data were split into two groups according to volunteer's height proximity to either 175 cm or 160 cm. The results indicated that the

group comprising the taller volunteers moved the seat slide, in average, 4 notches back from the neutral position and did not modify the shoulder belt anchor height. The group comprising the shorter volunteers moved the seat slide 1 notch back from neutral position and reduced the shoulder belt anchor height one notch. Both height groups set the same seat lift and seat back inclination. Initial neutral positions and height group dependent adjustments from the survey study and used to adjust seat and seatbelt anchor layout in the current simulation study are shown in TABLE II.

TABLE II. Survey results on preferred driving position used to set seat position and seatbelt anchors layout for AM50 and *Small* size driver FE models used in this study

	Initial Neutral Position	AM50	Small
Seat Slide (number of notches from front most)	8	12	9
Seat back Inclination (number of notches from front most)	4	3	3
Seat lift (mm above lowest)	16	10	10
Seatbelt anchor (number of notches from Highest)	0	0	1

Driver Models positioning and seatbelt fitting

The driver models were positioned on the seat by using a gravity drop-down method [28]. First, the human model with an initial UMTRI position was placed just above the un-deformed seat cushion. A simulation of a long event (of 1 second of duration) under the effect of a vertical 1g acceleration was conducted. In this simulation, few nodes from the spine, head, arms and legs were constrained in vehicle horizontal direction in order to keep control of the driver's posture. The driver model deformed the seat cushion and rebounded vertically until the driver model became steady. Thereafter, a second simulation was conducted in which the arms and feet were prescribed the motion needed to reach the steering wheels and the pedals. In this simulation, spinal nodes were also constrained in vertical direction. Finally, the seatbelt model was developed based on the positioned occupant model. The shoulder belt model was developed so its center line travelled from the upper to the lower slip-rings passing above the mid-clavicle, mid-sternum, and eight costochondral joint of the driver model. The lap belt was developed to connect the lower slip-ring with the fixed belt anchorage and passing above the left and right anterior-superior iliac anatomical landmarks. This positioning and belt fitting process was conducted for the AM50 and the *Small* models separately. Figure 1 shows an oblique image of the AM50 final position including the seatbelt. Lateral images of the final positions with the AM50 and the Small size models are included in Figures D6 and D7, respectively.

Crash Pulse

An acceleration pulse from a 56 km/h New Car Assessment Program full frontal crash test conducted with a mid-size sedan car similar to the vehicle model used in this study was downloaded from NHTSA database [29]. This pulse, shown in Figure 1, was prescribed to the vehicle model in longitudinal direction to simulate the same frontal crash conditions for all cases included in this study.

Simulation matrix

The above described driver FE models (Adult AM50, Elderly AM50 and Elderly *Small*), the four belt force limit settings (2, 3, 4 and 5kN) and the three airbag pressure settings (Low, Mid and High) were combined to conduct a total of 36 frontal crash simulations according to TABLE III.

III. RESULTS

TABLE III lists the case number (column 1), the driver model thoracic age setting and body size (columns 2 and 3) and the restraint systems settings (columns 4 and 5) for all the cases simulated. The table also includes the resulting peak values for chest deflection, chest excursion, and head displacement (columns 6 to 8), as well as the predicted number of fractured ribs (NFR) and the location of these (column 9). Chest deflection was measured as the change in percentage of the distance between the mid-sternal point and the eighth thoracic vertebra (T8). Initial distances were 212 and 196 mm for the AM50 and the *Small* models, respectively. Chest

excursion was measured as the forward displacement of T8. Head displacement was measured as the forward displacement of the centre of gravity of the head. A rib fracture was accounted for by means of an element elimination method applied to the rib cortical bone model shell elements. Such method identifies and deletes the elements that reach a predefined failure strain level during the simulated loading. In this study, 3% and 1.5% failure strain levels were set for the Adult and the Elderly thoracic settings, respectively (Figure 2.b).

TABLE III. Simulation matrix and results

Case No.	Simulation settings				Simulation results			
	Occupant model		Restraint systems		Chest def. (%)	Chest disp. (mm)	Head disp. (mm)	Number of fractured ribs and their locations
	Thorax age	Body size	Airbag pressure	Belt force limit (kN)				
1	Adult	AM50	Low	2	13.4	351	542	0
2				3	15.5	329	530	0
3				4	17.0	309	507	0
4				5	19.1	290	478	0
5			Mid	2	14.1	342	535	0
6				3	15.6	324	517	0
7				4	18.1	300	488	0
8				5	19.3	283	463	0
9			High	2	14.8	328	504	0
10				3	15.4	307	485	0
11				4	17.6	289	460	0
12				5	19.8	274	442	0
13	Elderly	Small	Low	2	12.1	294	439	0
14				3	14.5	275	421	2 (R1,R2)
15				4	17.5	256	397	8 (R1,R2,R3,L6,L7,L8,L9,L10)
16				5	20.6	239	377	10 (R1,R2,R3,R4,L1,L6,L7,L8,L9,L10)
17			Mid	2	12.7	286	411	0
18				3	15.1	267	395	2 (R1,R2)
19				4	18.1	248	374	8 (R1,R2,R3,L6,L7,L8,L9,L10)
20				5	21.3	233	358	11 (R1,R2,R3,R4,L1,L5,L6,L7,L8,L9,L10)
21			High	2	13.0	268	376	0
22				3	15.2	250	250	2 (R1,R2)
23				4	18.4	234	234	7 (R1,R2,R3,L6,L7,L8,L9)
24				5	22.6	221	221	10 (R1,R2,R3,R4,L1,L6,L7,L8,L9,L10)
25		AM50	Low	2	15.5	355	541	0
26				3	17.6	333	525	3 (R1,R2,L7)
27				4	22.2	309	503	9 (R1,R2,R3,L1,L6,L7,L8,L9,L10)
28				5	23.5	294	483	9 (R1,R2,R3,L1,L6,L7,L8,L9,L10)
29			Mid	2	14.7	344	533	0
30				3	16.9	320	509	1 (R1)
31				4	20.8	300	482	8 (R1,R2,R3,L6,L7,L8,L9,L10)
32				5	23.1	287	461	9 (R1,R2,R3,L1,L6,L7,L8,L9,L10)
33			High	2	16.0	332	510	0
34				3	17.8	313	490	3 (R1,R2,L7)
35				4	22.2	295	464	9 (R1,R2,R3,L5,L6,L7,L8,L9,L10)
36				5	24.6	279	443	11 (R1,R2,R3,L1,L2,L5,L6,L7,L8,L9,L10)

The results show that, for a given occupant model and airbag setting, as belt force limit increased, chest excursion decreased and chest deflection increased (e.g. Cases 5 to 8). For a given occupant model and belt force limit, as airbag pressure settings increased, chest and head displacements decreased but chest deflections did not necessarily increase (e.g. Cases 2, 6 and 10). For equal restraint systems setting, *Small* size model sustained lower chest excursions, head displacements and chest deflections than the AM50 models. These lower values did not imply lower numbers of predicted fractures (e.g. Case 19 and 31). The simulations with the

Adult AM50 model predicted no rib fracture. The simulations with thoracic properties representative of an Elderly, predicted no fracture for the 2 kN belt force limit, 1 to 3 fractures for the 3 kN limit, and 7 or more fractures for the 4 and 5 kN limits. When low numbers of rib fractures were predicted, these tended to occur at the upper part of the ribcage on the right side shoulder engaged by the belt (e.g. Case 14). For larger numbers of fractures, these occurred on the lower left part of the ribcage in addition to those on the upper part (e.g. Case 15).

Effect of occupant body size and age

Images of body kinematics and its interaction with the restraint systems at maximum body forward displacement (90 ms) for the three driver models with a 4 kN belt force limit and Mid airbag setting are shown in Figure 3. Complete sequences of images from these cases are shown in Figure D6 to Figure D8 (Appendix D).

Adult AM50 (Case 7) Elderly *Small* (Case 19) Elderly AM50 (Case 31)

Figure 3. Body kinematics for three driver models (Adult AM50, Elderly *Small*, and Elderly AM50) with a 4kN belt force limit and Mid airbag setting

Figure 4 shows belt and airbag loads, chest deflection and the sequence of rib fractures for the same cases presented in Figure 3. The simulations with the Adult AM50 model predicted no single rib fracture. Both the Elderly *Small* and Elderly AM50 models predicted 8 rib fractures. The majority of rib fractures occurred before the torso entered into full contact with the inflated airbag.

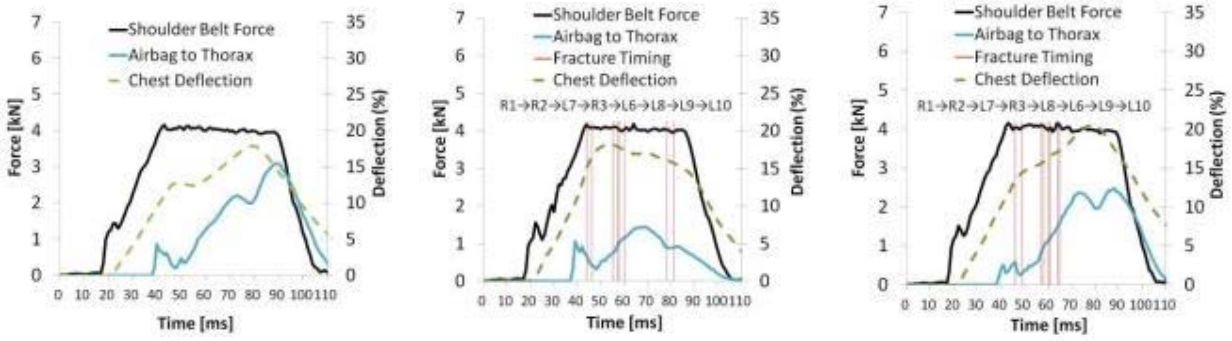

Adult AM50 (Case 7) Elderly Small (Case 19) Elderly AM50 (Case 31)

Figure 4. Belt load, airbag load, chest deflection and sequence of rib fractures for three different driver models (Adult AM50, Elderly *Small*, and Elderly AM50) with a 4kN belt force limit and Mid airbag setting

Figure 5 shows the NFR as a function of chest deflection for all simulated cases. The results show that predicted number of rib fractures increased with chest deflection for both Elderly Small and Elderly AM50 models. For a given level of injury of 3 rib fractures (which corresponds with a threshold for severe thoracic skeletal AIS3 injuries), chest deflections of 15.3 % (30 mm) and 18% (38 mm) were obtained for the *Small* and the AM50 models, respectively.

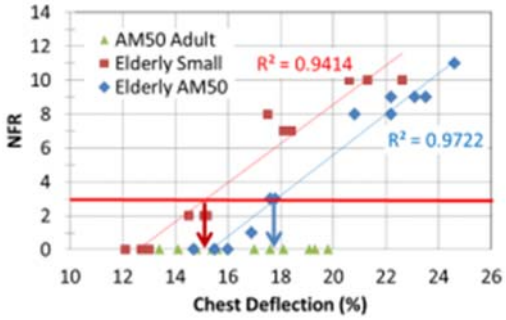

Figure 5. NFR vs Chest deflection for all simulated cases with the Adult AM50 (triangular markers), the Elderly *Small* (square markers) and the Elderly AM50 (rhomboidal markers) models. A red line is drawn at NFR=3

Effect of belt force limit

Figure 6 and Figure 7 show the results of varying belt force limits (2 to 5 kN) with two Elderly driver models (*Small* and AM50) and Mid airbag. Figure 6 shows images of body kinematics and its interaction with the restraint systems. Reduced belt force limits decreased chest deflections and increased body forward displacement. Figure 7 presents belt loads, airbag loads and chest deflections. This increase led to head strikethrough against the upper part of the steering wheel in two of the cases with the AM50 (Cases 29 and 30).

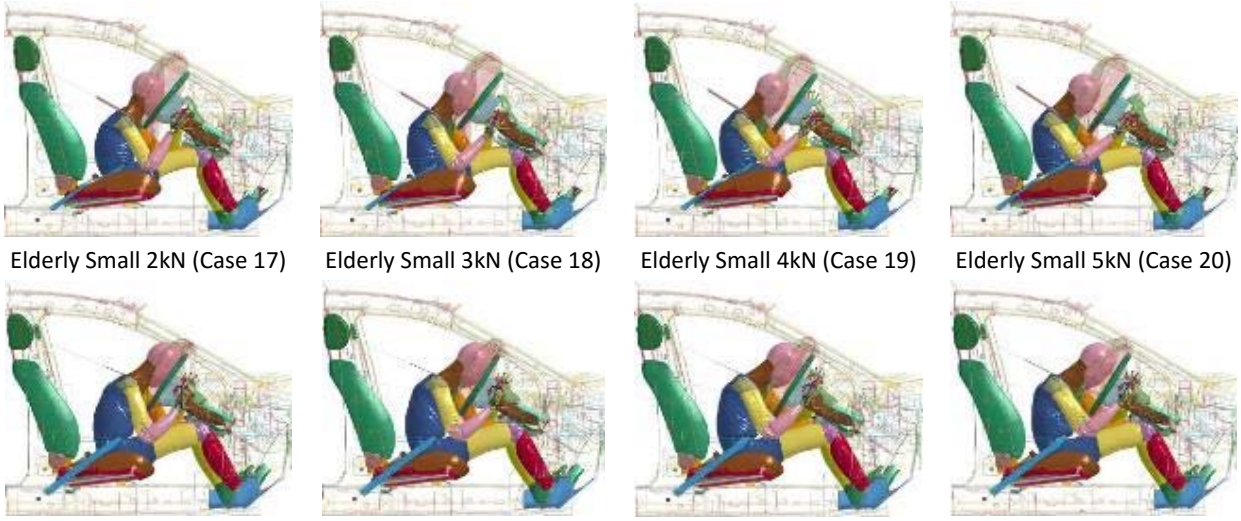

Elderly Small 2kN (Case 17) Elderly Small 3kN (Case 18) Elderly Small 4kN (Case 19) Elderly Small 5kN (Case 20)

Elderly AM50 2kN (Case 29) Elderly AM50 3kN (Case 30) Elderly AM50 4kN (Case 31) Elderly AM50 5kN (Case 32)

Figure 6. Body kinematics for two Elderly driver models (*Small* and AM50) with variable belt force limits (2 to 5 kN) and Mid airbag settings

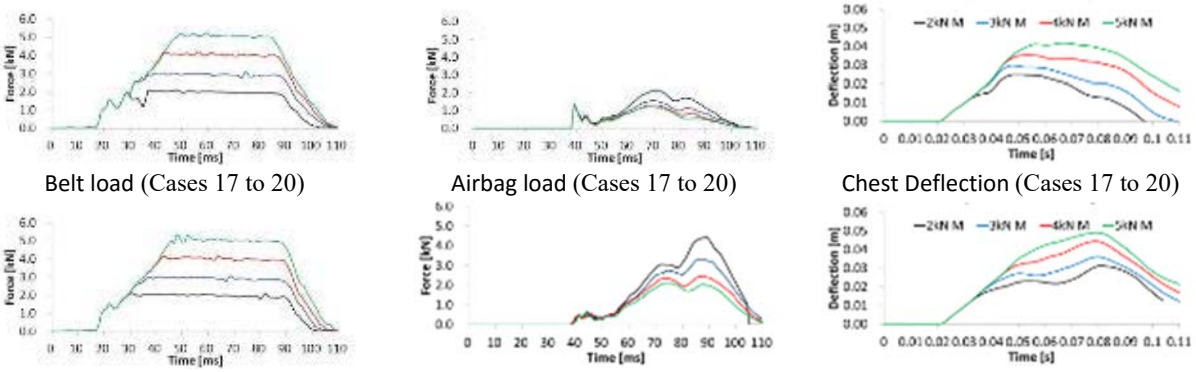

Belt load (Cases 17 to 20) Airbag load (Cases 17 to 20) Chest Deflection (Cases 17 to 20)

Belt load (Cases 29 to 32) Airbag load (Cases 29 to 32) Chest Deflection (Cases 29 to 32)

Figure 7. Belt loads (left column), airbag loads (middle column), and chest deflections (right column) for two Elderly driver models (*Small* and AM50) with variable belt force limits (2 to 5 kN) and Mid airbag settings

Effect of air bag pressure setting

Figure 8 shows the results of varying airbag pressure settings (Low, Mid, High) with the Elderly *Small* and the Elderly AM50 driver models for a single (3 kN) belt force limit. For increasing airbag pressure settings, chest and head displacement decreased for both driver models, but the effect on chest deflections was minimal. Head strikethrough occurred for one case with the AM50 model (Case 26).

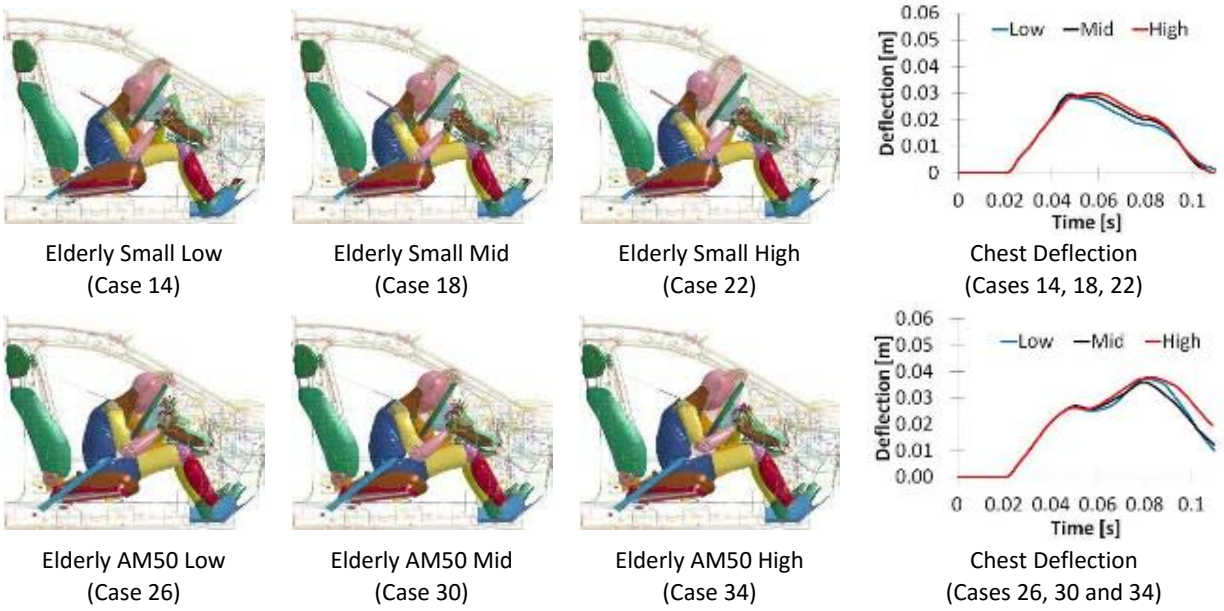

Elderly Small Low (Case 14) | Elderly Small Mid (Case 18) | Elderly Small High (Case 22) | Chest Deflection (Cases 14, 18, 22)

Elderly AM50 Low (Case 26) | Elderly AM50 Mid (Case 30) | Elderly AM50 High (Case 34) | Chest Deflection (Cases 26, 30 and 34)

Figure 8. Body kinematics (columns 1 to 3) and chest deflection (column 4) for two Elderly driver models (*Small* and AM50) with variable airbag pressure settings (Low, Mid and High) and 3kN belt force limit.

Rib fracture patterns and head strikethrough events

Figure 9 summarises the predicted number of fractured ribs (NFR) and the location of these, peak head displacement and occurrence of head strikethrough for all the 36 cases simulated with the Adult AM50 (Left block), the Elderly Small (Middle block) and the Elderly AM50 models (Right block) for all restraint systems settings. The NFR is colour coded; green for NFR lower than 3 and orange for NFR 3 or higher. The cases in which head strikethrough occurred are highlighted in red.

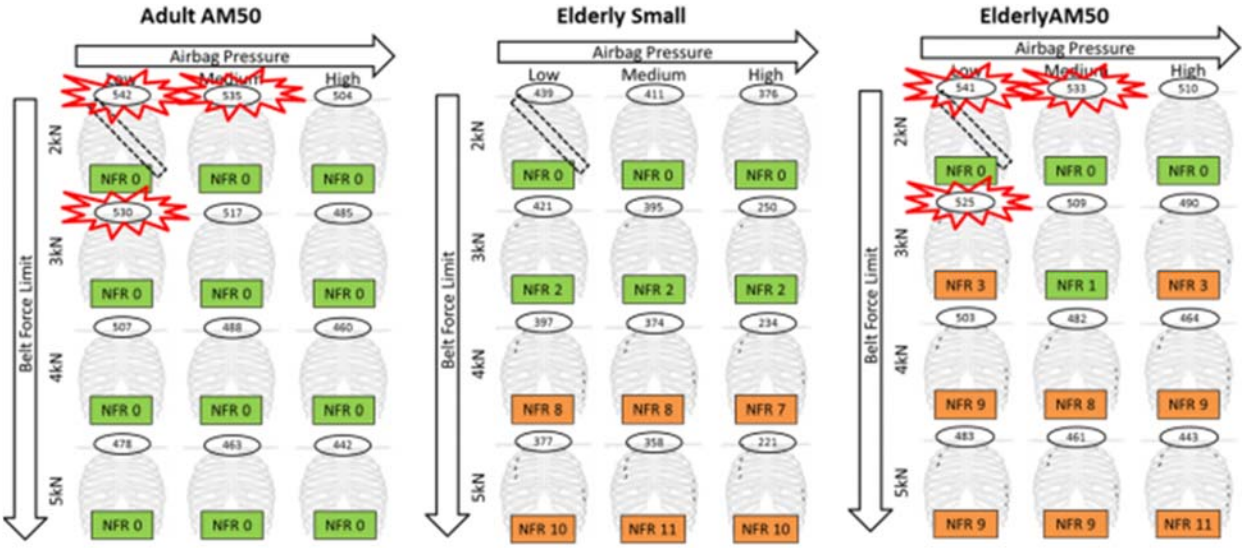

Figure 9. Number of fractured ribs and peak head forward displacement for all occupant and restraint systems settings presented in this study. Head strikethrough cases are highlighted with a red sign.

IV. DISCUSSION

In the simulations presented in this study, the HIII AM50 dummy model (Figure C5) and the AM50 human models (Figures D6 to D8) were restrained differently under similar crash conditions and restraint systems settings. While the HIII model appeared to be optimally restrained, the human models sustained lack of torso rotation and excessive excursion. This sub-optimal restraint may have contributed to produce the large numbers of rib fractures predicted for some of the cases with elderly models (Figure 9). In comparison to the HIII model, more extended lower extremities and their interaction with the pedals and knee bolster, softer interaction between the abdominal region and the lap belt, and increased spinal flexibility in the human models are some of the factors that may have contributed to the sub-optimal restraint. It is however noted that forward excursions in the cases simulated with the Adult AM50 model in the current study (250-350 mm for cases 5 to 8 in Figure G16) were in a similar range as those in a comparable study using different Adult AM50 human and vehicle FE models (300-400 mm for cases 6 to 9 in [13]). This suggests that the increased occupant excursion with respect to the HIII dummy may not be specific of the human models or vehicles in the current study. Hence, suggesting that optimal restraint of HIII dummies may not be enough to ensure optimal restraint of human-like occupants, which calls for the incorporation of human FE models in the refinement of future restraints systems.

The simulated crashes with human models predicted no single rib fracture with the Adult AM50 model and high numbers of rib fractures with the Elderly models when the belt force limits were 4 kN or higher (Figure 9). In general, these predictions are consistent with several accident data studies that have suggested that belt force limits lower than 4 kN may be required to prevent high numbers of rib fractures in the elderly [30-32]. However, the validity of the exact number of predicted fractures is more uncertain. The element elimination approach utilised to predict fractures deletes any element of the rib cortical bone model that reaches a pre-determined strain level (1.5% for elderly) during a calculation. As rib elements are deleted, the contribution of the fractured ribs to maintain structural thoracic integrity is reduced, transferring additional loads to the ribs adjacent to those already fractured. While accounting for this effect may be important for the accurate quantification of rib fractures, the method may also produce rib load shifts that lead to localised raise of strains and, consequently, to over prediction of rib fractures. Incorporating probabilistic approaches may help to increase the confidence in the quantified numbers of predicted rib fractures in future studies [33][34].

Occupant age and body size are regarded as two important factors that may influence thoracic injury output in frontal crashes. While accident data studies clearly show that age is a crucial factor in frontal crashes [1][4][35], evidences on the effect of body size in thorax injury risks seem to be less conclusive [1][6]. The importance of considering body size is usually driven by frontal crash tests dummies of smaller size which commonly predict increased thoracic injury risks compared to average size dummies [36]. The current simulation study predicted no fractures with Adult thoracic properties and increasingly higher number of fractures with Elderly properties for increasing belt force limits (Figure 9). The results also revealed that, despite the similar levels of fractures predicted with the Small and the AM50 models, these were produced under different interaction mechanisms with the restraint systems (e.g. Case 19 and Case 31 in Figure 4) and at different levels of chest thoracic deflection (Figure 5). The Small model sustained less chest and head forward displacements and lower airbag to thorax contact forces. These differences highlight the need to incorporate human FE models of different body sizes that enable optimisation of restraint systems also for populations not covered by the dummies.

The combination of belt force limiter with an airbag has been shown to effectively reduce thoracic injury risk in frontal crashes [37][38]. Furthermore, accident data studies have suggested the benefits of a 4 kN belt force limit [31][39]. Some of these studies have also suggested that thoracic injuries for senior occupants would be further reduced with belt forces lower than 4 kN [30-32]. A recent series of frontal crash tests with an AM50 THOR dummy and variable belt force limits identified that reducing the belt force limit from 4 to 3 kN without modifying the airbag, decreased thoracic injury risk indicators [12]. However, this reduction of thoracic injury risk was accompanied by an increase of head forward displacement that led to head strikethrough mechanism [12]. The simulations with the Elderly AM50 model presented in this work are consistent with both the accident studies considering ageing [40] and the THOR dummy tests [12]. The simulation results showed a large drop in the number of predicted rib fractures (from more than 7 fractures to less than 3) when belt force limit was reduced from 4 to 3 kN. Interestingly, this reduction was also associated with an increase of head forward travelling and a head strikethrough mechanism similar to that identified in the tests [12]. In addition, the

simulations with the small size model allow suggesting that smaller drivers may be less likely to encounter the potential head strikethrough.

The introduction of airbags has contributed to a significant decline in the number of head and facial injuries [41]. However, a concomitant reduction in the number of thorax injuries from the same studies is less clear [1][41]. The simulation results in the current study are somehow consistent with such field observations. On one hand, increased airbag pressure settings did not considerably affect thoracic excursion, but did affect head forward displacement. Furthermore, head strikethrough was prevented in the cases with larger excursion by increasing airbag pressure (Figure 9). On the other hand, sequential analysis (Figure 3) showed that, when a large number of fractures occurred in the simulations, these mainly occurred before the thorax entered into full contact with the deployed airbag. These findings suggest that, while the airbag seems to be indispensable for head injury protection, more effective thoracic protection strategies may be achieved on belt design, rather than airbag design. The findings also highlight the importance of finding a balance between restraint from the seat belt and the airbag and call for further studies on the need of occupant specific restraints.

V. LIMITATIONS

The human models used in this study incorporate detailed geometry of the thoracic inner organs. The contribution of these organs to thoracic effective stiffness in compression was validated [18]. In addition, the liver model was developed and validated in detail based on experimental data [42]. However, the validation of other organs such as lungs, heart, or major vessels commonly involved in traffic related thoracic injuries, is limited. Hence, detailed inner organ injury mechanisms and risks were not considered in this study. To overcome this limitation, it was assumed that rib fractures are a good indicator of other thoracic injuries [43]. Nevertheless, further experimental and modeling work is required to enhance the validation of models so that thoracic inner organs injury mechanisms and risks can be incorporated in future studies.

The generic vehicle and restraints systems FE models used in this study have been designed with extensive component experimental data. In addition, an evaluation of the models was conducted against white-body sled test with a HIII (Appendix C). Nevertheless, the vehicle model cannot be considered a thoroughly validated vehicle model and the restraint systems may not be representative of current actual vehicles. Current real vehicles and restraints systems undergo development processes more rigorous than the conducted in this study. Hence, the results of this study may likely be biased towards over-prediction of rib fractures and additional work to incorporate state-of-the-art restraints systems is needed

This study is limited to a single 56 km/h equivalent barrier crash pulse representative of full overlap frontal crash tests and may not necessarily be representative of the crash conditions that most commonly cause thoracic injuries in real-world accidents. Similarly, the limited number of driver model positions and the restraint systems settings defined for the study are insufficient to allow generalising the conclusions of this study.

VI. CONCLUSIONS

The effect of different combinations of seatbelt and airbag loads on the number and locations of rib fractures has been evaluated in simulated full frontal crashes with a human FE model that accounts for age-dependent thorax fragility and reduced body size. Considering the above mentioned limitations and restricted to the simulated conditions, the following is concluded:

Elderly *Small* occupant sustained less forward motion and chest deflections than the Elderly AM50. Despite these reduced values, for a given belt force limit, similar levels of skeletal fractures were predicted. This highlights the benefit of incorporating human FE models of different body sizes that enable optimization of restraint systems also for populations not covered by the dummies.

The majority of rib fractures occurred along the belt path, initiating on the engaged shoulder site and propagating to the lower part of the thorax. Sequential analysis showed that the fractures occurred before the torso entered into full contact with the inflated airbag. These findings suggest that more effective elderly thoracic protection strategies may be achieved on belt design, rather than airbag design.

Reduced belt force limits lowered the number of predicted rib fractures in the elderly. However, this reduction was achieved at the cost of increasing body forward excursion which, in some cases, led to head strikethrough mechanism. These mechanisms were prevented for both Small and AM50 occupants with a slight

increase of airbag pressure. This suggests that if elderly specific restraint systems were to be developed, the design must be guided by the principle of reducing thoracic load in addition to compensating for possible increase of head forward displacement.

In summary, this study highlights the importance of accounting for age-dependent thoracic fragility and body size in search of optimal thoracic protection for diverse populations, including the elderly. In addition, as crash mitigation technologies penetrate the market, this study provides a baseline to incorporate thoracic injury risk evaluations into integrated safety research strategies.

VII. REFERENCES

[1] Carroll J, Adolph T, et al. Overview of serious thorax injuries in European frontal car crash accidents and implications for crash test dummy development. *Proceedings of IRCOBI Conference*, 2010, Hanover, Germany.

[2] Yaguchi M, Omoda Y, Ono K, Masuda M, and Onda K. Traffic accident analysis towards the development of an advanced frontal crash test dummy indispensable for further improving vehicle occupant protection performance. *Proceedings of 22nd ESV Conference*, 2011, Washington D.C, USA.

[3] Japanese Police. "Annual report on road traffic fatal accidents and traffic law enforcement violations [in Japanese]", 2013. Internet http://www.npa.go.jp/toukei/index.htm#koutsuu. [2016 February 20th].

[4] Kent R, Patrie J, Poteau F, Matsuoka F, and Mullen C. Development of an age-dependent thoracic injury criterion for frontal impact restraint loading. *Proceedings of 18th ESV Conference*, 2003, Nagoya, Japan.

[5] Wang S. Population variability: influence of crash injury outcomes. *Proceedings of JSAE Annual Congress Forum*, 2013, Yokohama, Japan.

[6] Hynd D, Carroll J, Cuerden R, Kruse D, and Boström O. Restraint system safety diversity in frontal impact accidents. *Proceedings of IRCOBI conference*, 2012, Dublin, Ireland.

[7] United Nations Department of Economic and Social Affairs. "World Population Prospects: The 2012 Revision", 2012. Internet http://esa.un.org/wpp. [2016 February 20th].

[8] Research Institute of Human Engineering Quality of Life. "Japanese Body Size Data Book 2004–2006", 2008. Internet http://www.hql.jp/database/size2004. [2015 April 18th].

[9] Mendoza-Vazquez M. Thoracic injuries in frontal car crashes: risk assessment using a finite element human body model, 2014. PhD Thesis, Chalmers University of Technology.

[10] Bean J D, Kahane C J, et al. Fatalities in Frontal Crashes Despite Seat Belts and Air Bags–Review of All CDS Cases–Model and Calendar Years 2000-2007–122 Fatalities, 2009.

[11] Rudd R W, Bean J, et al. A study of the factors affecting fatalities of air bag and belt-restrained occupants in frontal crashes. *Proceedings of 21st ESV Conference*, 2009, Stuttgart, Germany.

[12] Sunnevång C, Hynd D, Carroll J, and Dahlgren M. Comparison of the THORAX Demonstrator and HIII sensitivity to crash severity and occupant restraint variation. *Proceedings of IRCOBI Conference*, 2014, Berlin, Germany.

[13] Kitagawa Y and Yasuki T. Correlation among seatbelt load, chest deflection, rib fracture and internal organ strain in frontal collisions with human body finite element models. *Proceedings of IRCOBI Conference*, 2013, Gothenburg, Sweden.

[14] Chang C-Y, Rupp J D, Reed M P, Hughes R E, and Schneider L W. Predicting the effects of muscle activation on knee, thigh, and hip injuries in frontal crashes using a finite-element model with muscle forces from subject testing and musculoskeletal modeling. *Stapp Car Crash Journal*, 2009

[15] Iwamoto M, Nakahira Y, Kimpara H, and Min K. Development of a Finite Element Model of 5th Percentile Female with Multiple Muscles and Its Application to Investigation on Impact Responses of Elderly Females. *Proceedings of 23rd ESV Conference*, 2013, Seoul, Republic of South Korea.

[16] Schoell S L, Weaver A A, Vavalle N A, and Stitzel J D. Age-and sex-specific thorax finite element model development and simulation. *Traffic injury prevention*, 2015. 16(sup1): p. S57-S65

[17] Ito Y, Dokko Y, Motozawa Y, Mori F, and Ohashi K. Kinematics Validation of Age-Specific Restrained 50 th Percentile Occupant FE Model in Frontal Impact, 2012. SAE Technical Paper.

[18] Antona-Makoshi J, Yamamoto Y, et al. Age-dependent factors affecting thoracic response: a finite element study focused on Japanese elderly occupants. *Traffic injury prevention*, 2015. 16(sup1): p. S66-S74

[19] Stein I and Granik G. Rib structure and bending strength: an autopsy study. *Calcified tissue research*, 1976. 20(1): p. 61-73

[20] Ito O, Dokko Y, and Ohashi K. Development of adult and elderly FE thorax skeletal models, 2009. SAE Technical Paper.
[21] Kato R, Yamamoto Y, et al. A Methodology to Develop Rib Finite Element Models that account for Cortical Bone Thickness *Proceedings of Annual JSAE Congress*, 2014, Yokohama, Japan.
[22] Kemper A R, McNally C, et al. Material properties of human rib cortical bone from dynamic tension coupon testing. *Stapp Car Crash Journal*, 2005
[23] Yamada H and Evans F G, "Strength of biological materials", Williams & Wilkins: Baltimore, USA, 1970.
[24] McElhaney J H, Roberts V L, and Hilyard J F, "Handbook of human tolerance", Japan Automobile Research Institute: Tsukuba, Japan, 1976.
[25] Kroell C K, Schneider D C, and Nahum A M. Impact tolerance and response of the human thorax II, 1974. SAE Technical Paper.
[26] Shaw G, Parent D, et al. Impact response of restrained PMHS in frontal sled tests: skeletal deformation patterns under seat belt loading. *Stapp Car Crash Journal*, 2009
[27] Masuda M, Yaguchi M, and Ono K. Repeatability and sensitivity to seat-position of THOR-NT and Hybrid III based on HyGe sled tests. *Proceedings of IRCOBI conference*, 2008, Bern, Switzerland.
[28] Antona J, Ejima S, and Zama Y. Influence of the driver conditions on the injury outcome in front impact collisions. *International Journal of Automotive Engineering*, 2011. 2(2)
[29] National Highway Traffic Safety Administration. "Vehicle Crash Test Database: New Car Assessment Program", 2015 Internet http://www.nhtsa.gov/Research/Databases+and+Software. [2016 February 20th].
[30] Forman J, Lessley D, et al. Thoracic response of belted PMHS, the Hybrid III, and the THOR-NT mid-sized male surrogates in low speed, frontal crashes. *Stapp Car Crash Journal*, 2006. 50: p. 191
[31] Foret-Bruno J-Y, Trosseille X, et al. Comparison of Thoracic Injury Risk in Frontal Car Crashes for Occupant Restrained without Belt Load Limiters and Those Restrained with 6 kN and 4 kN Belt Load Limiters. *Stapp Car Crash Journal*, 2001. 45: p. 205-224
[32] Mertz H J and Dalmotas D J. Effects of shoulder belt limit forces on adult thoracic protection in frontal collisions. *Stapp Car Crash Journal*, 2007. 51: p. 361-380
[33] Boström O, Motozawa Y, Oda S, Ito Y, and Mroz K. Mechanism of reducing thoracic deflections and rib strains using supplemental shoulder belt during frontal impacts. *Proceedings of 23th ESV Conference*, 2013,
[34] Forman J L, Kent R W, et al. Predicting rib fracture risk with whole-body finite element models: development and preliminary evaluation of a probabilistic analytical framework. *Proceedings of AAAM Conference*, 2012, Seattle, USA.
[35] Shimamura M, Ohhashi H, and Yamazaki M. The effects of occupant age on patterns of rib fractures to belt-restrained drivers and front passengers in frontal crashes in Japan. *Stapp Car Crash Journal*, 2003. 47: p. 349
[36] Ridella S A, McCann M J, Turnbull R C, and Bayley G S. Development of restraint systems with considerations for equality of injury risk. *Proceedings of 19th ESV Conference*, 2005, Washington D.C., USA.
[37] Kallieris D, Rizzetti A, et al. On the synergism of the driver air bag and the 3-point belt in frontal collisions. *Proceedings of Stapp Car Crash Conference*, 1995,
[38] Augenstein J, Perdeck E, et al. Injury Patterns Among Belted Drivers Protected by Air Bags in 30 to 35 mph Crashes, 1999. SAE Technical Paper.
[39] Lu H, Andreen M, et al. Safety Belt and Occupant Factors Influencing Thoracic & Upper Abdominal Injuries in Frontal Crashes, 2011. SAE Technical Paper.
[40] Foret-Bruno J, Trosseille X, et al. Thoracic injury risk in frontal car crashes with occupant restrained with belt load limiter, 1998. SAE Technical Paper.
[41] Knack S S R, Pastor C, Hynd D and Owen C. . Final Report of Work Package 1: Frontal Accident Analysis Study. EC project report, 2003.
[42] Sato F, Yamamoto Y, et al. Hyper-viscoelastic response of perfused liver under dynamic compression and estimation of tissue strain thresholds with a liver finite element model. *Proceedings of IRCOBI Conference*, 2013, Gothenburg, Sweden.
[43] Wanek S and Mayberry J C. Blunt thoracic trauma: flail chest, pulmonary contusion, and blast injury. *Critical care clinics*, 2004. 20(1): p. 71-81
[44] Hamzah M, Subit D, et al. An inverse finite element approach for estimating the fiber orientations in intercostal muscles. *Proceedings of IRCOBI Conference*, 2013, Gothneburg, Sweden.
[45] Subit D and Salzar R. Ribcage kinematics under belt loading in intact, denuded and eviscerated conditions. *Proceedings of Annual JSAE Congress*, 2014, Yokohama, Japan.

[46] Zama Y, Antona J, et al. Development of finite element human model for events of frontal impact. *Proceedings of Annual JSAE Congress*, 2010, Yokohama, Japan.
[47] Rhule H H, Maltese M R, et al. Development of a new biofidelity ranking system for anthropomorphic test devices. *Stapp Car Crash Journal*, 2002. 46: p. 477-512
[48] Sugimoto T and Yamazaki K. First results from the JAMA human body model project. *Proceedings of 19th ESV Conference*, 2005, Washington DC, USA.
[49] Mohan P, Park C-K, et al. LSTC/NCAC dummy model development. *Proceedings of 11th International LS-Dyna Users Conference*, 2010, Detroit MI, USA.

APPENDIX A: Summary of human FE model development, validation process and results and model availability

A model of the thorax was developed from CT images of 71-year-old postmortem human subject (PMHS). The PMHS body size (161cm, 60 kg) and ribcage dimensions fell within average Japanese elderly male population. The model included the ribcage, the spine, the inner organs and the surrounding thoracic flesh/skin. The ribs were developed according to a methodology proposed by [21]. This methodology consists of extracting the geometry of each rib and its variable cortical bone thickness from the CT images. Thereafter, a mesh of each rib is constructed and the corresponding measured thickness is assigned to each element of the mesh. In total, the methodology was applied to develop nine ribs model (2^{nd} to 10^{th} ribs). These rib models were validated by simulating bending tests conducted with the corresponding ribs collected from the elderly PMHS [21]. Since this model development method and validation was not applicable to short and straight ribs, the 1^{st}, 11^{th} and 12^{th} ribs were simply modelled by assigning uniform cortical bone thickness and the same material properties as the 2^{nd} to 10^{th} ribs. Besides the ribs, other thoracic components such as the costal cartilage and the intercostal muscles were also validated against component test data obtained from the PMHS specimen [44]. The liver model was carefully validated with porcine liver static and dynamic compression tests [42]. Other inner organs were assigned properties from tissue coupon tests from the literature. The validated components were assembled. This assembly was validated by simulating sub-injurious table top tests under different thoracic tissue conditions (intact, eviscerated, and denuded) conducted with the elderly PMHS [45]. This was done to confirm that the contribution of the flesh, the inner organs and the ribcage to thoracic structural stiffness in compression was similar to that measured in the experiments [18]. Thereafter, different components of the rib cage and the thoracic flesh materials were assigned age-dependent properties based on experimental data from the literature. These properties included rib cortical bone thickness [19][20], material properties [20][21], and ultimate strain [22], as well as costal cartilage material properties [23] and muscle/flesh material properties in tension and compression [23][24]. The validated thorax model was merged with the head and the extremities of a full scale model previously developed JAMA model [46]. This full body model comprised a total of 684,074 elements. The full body model geometry was linearly scaled up by applying a scaling factor based on body height of 1.09 in X, Y and Z directions. In doing so, two body size versions were created: the original 161 cm/60 kg and the 175 cm/77 kg. The AM50 size model with thoracic settings corresponding with an Adult (45 years) and Elderly (75 years) person was validated against existing biomechanical data from the literature. These data included age-dependent corridors developed from hub-to-thorax impact tests with PMHS [17][25] and frontal impact sled PMHS test data [26].

The results from the validation of the AM50 size model with age-dependent settings against PMHS data are summarised in Figure A1. Hub impactor simulation force-deflection results (Figure A1, above) show that the models with Elderly and Younger properties were in agreement with experimental one standard deviation age-dependent corridors. The model with Elderly and Younger properties predicted 12 and 2 rib fractures, respectively. Sled tests simulation results (Figure A1, below) show head and spine trajectories, shoulder belt loads, and ribcage multi-point deflection from the simulations in comparison to the corresponding experimental measures [26]. Trajectories of the head and the spine in x, y, and z directions were objectively evaluated according to a four level (Poor, Moderate, Good, Excellent) bio-fidelity ranking system proposed by [47]. The results (Rhule scores and ranks presented in the lower left part of the image) show that head and spinal motions tended to score Good to Excellent Similarly, shoulder belt loads (Good) and thoracic multi-point deflections (Excellent) for both Elderly and Younger settings presented in Figure A1 were in agreement with the experiments. Under these conditions, Elderly setting predicted 10 fractures (5 on each side of the ribcage) and Younger setting 2 rib fractures.

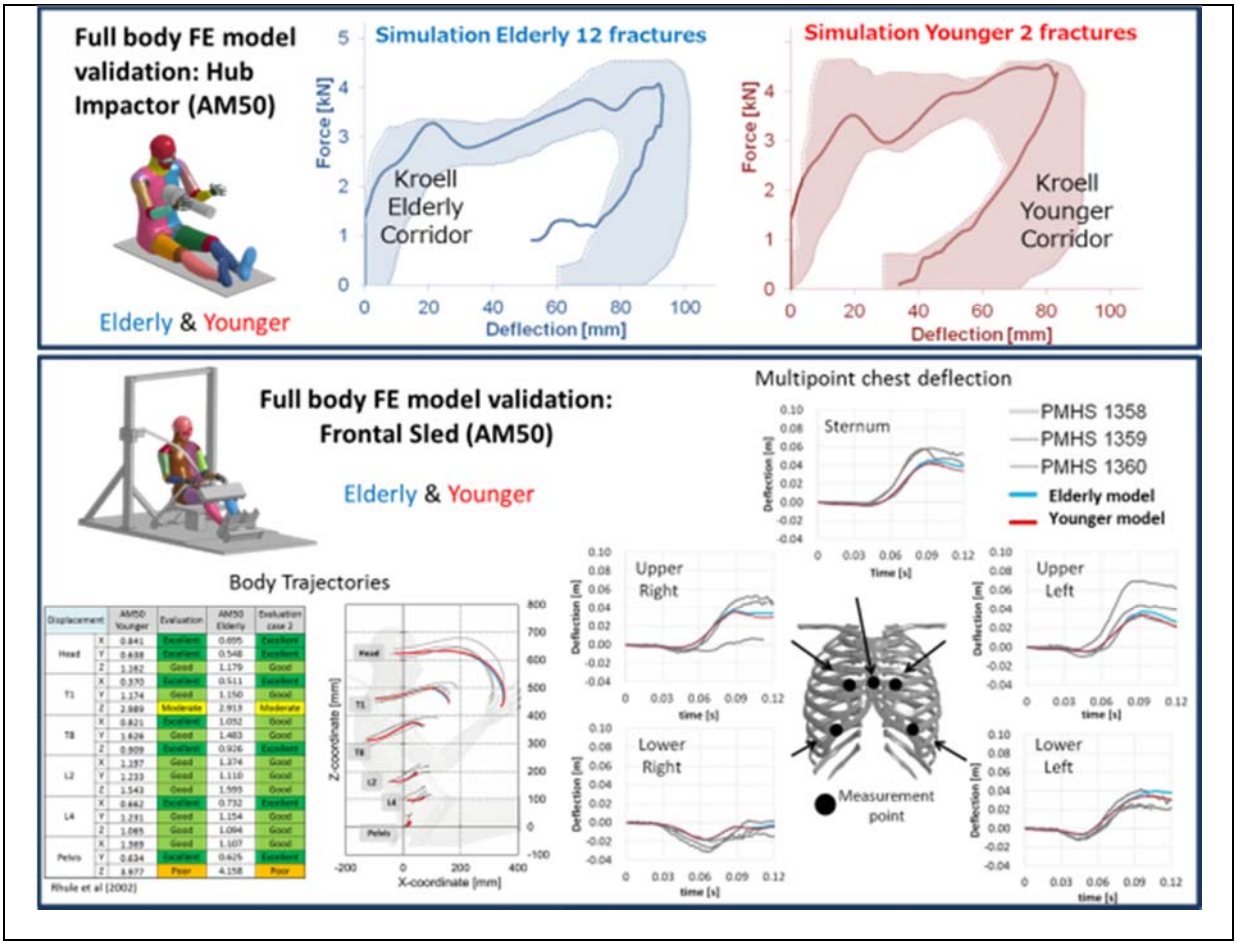

Figure A1. Summary of human body FE model validation results

The human models described have been developed within the frame of a research plan by the JAMA initiated in 2004 which has involved Japanese automobile makers, related research institutions and academia [48]. The models have been developed to support industry in the development of safer automobiles, but could potentially become a useful tool for other impact biomechanics research purposes and institutions [48]. The availability of the models for research may be possible upon consultation with the JAMA.

APPENDIX B: Real mid-size sedan car measurements for definition of vehicle FE model components layout

Figure B2 shows a schematic illustration of different vehicle components and measurements taken manually from a real mid-size sedan vehicle. The figure also includes a description of each of these measurements and the actual values measured. These values were used to set neutral positions for seat, seatbelt anchor points, knee bolster and pedals. the layout of the vehicle interior FE model.

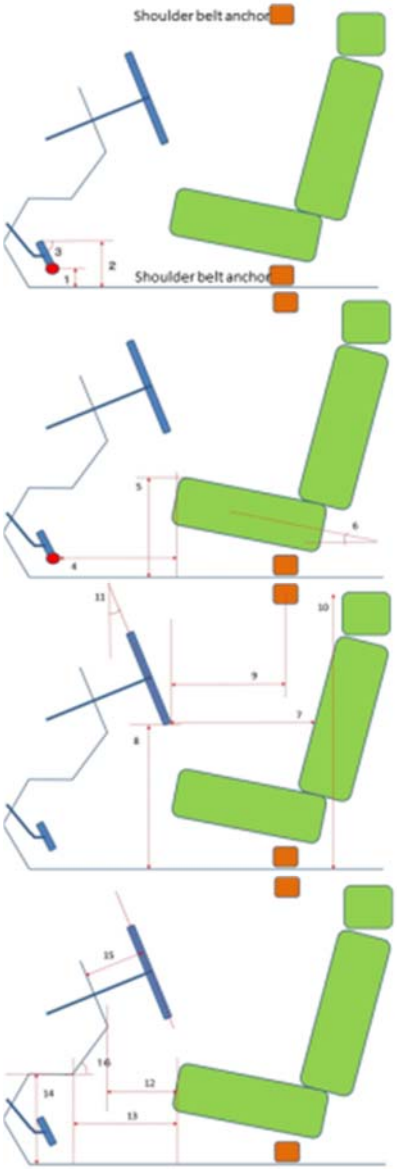

Measurement description	Measure
1. Foot pedal vertical distance from floor	124 mm
2. Foot pedal vertical distance from floor	170 mm
3. Foot pedal angle with respect to floor	45 deg.
4. Foot pedal to seat cushion horizontal distance	488 mm
5. Seat surface front end vertical distance from floor	290 mm
6. Seat surface angle with respect to floor	19 deg.
7. Steering rim lower end to seat back horizontal distance	560 mm
8. Steering rim lower end vertical distance from floor	460 mm
9. Steering rim lower end to shoulder belt anchor point horizontal distance	541 mm
10. Shoulder belt anchor vertical distance from floor	925 mm
11. Steering rim angle with respect to floor	66 deg.
12. Knee pad higher end to seat cushion horizontal distance	264 mm
13. Knee pad lower end to seat cushion horizontal distance	381 mm
14. Knee pad lower end vertical distance from floor	286 mm
15. Instrument panel to steering rim horizontal distance	193 mm
16. Knee pad angle with respect to floor	49 deg.

Figure B2. Vehicle layout measurements

APPENDIX C: Evaluation of Car Interior Sled-type model against frontal sled-test with HIII

The JARI vehicle interior FE model utilised in this study is shown in Figure C3. The model was evaluated by simulating a white body sled test with a HIII 50th percentile male ATD in the driver position [27]. In the white body sled test, a sinusoidal wave 55 km/h equivalent barrier speed was used. In the simulation, the acceleration pulse from the sled test was input as a prescribed acceleration to the floor of the vehicle interior model. In the simulation, the HIII 50th percentile male ATD was represented by the HIII 50th percentile male model distributed by LSTC [49]. Output data were the seat belt forces and HIII chest, head and pelvis accelerations, and the chest compression.

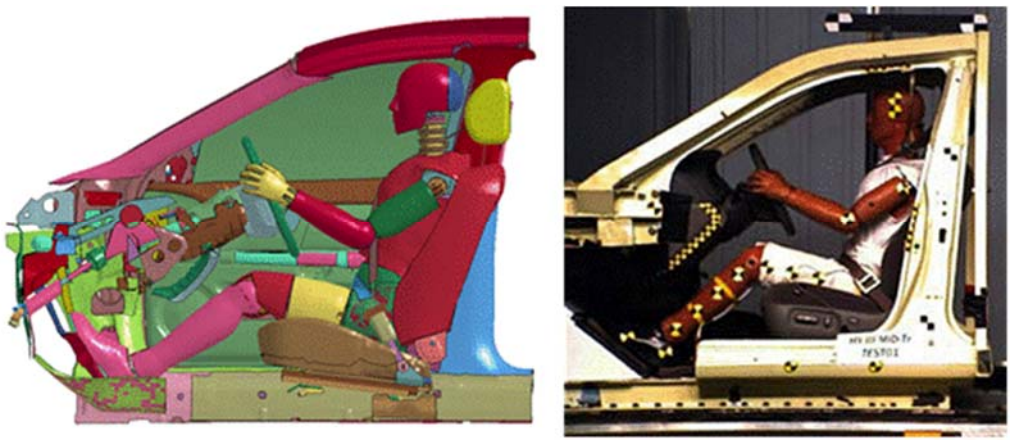

Figure C3. Simulation model and white body sled test for JARI car interior model evaluation

As shown in Figure C4, the compared signals reached similar levels and have similar shapes. Thus, the car interior model can be considered representative of the interior of a mid-size sedan while restraining a 50th percentile HIII.

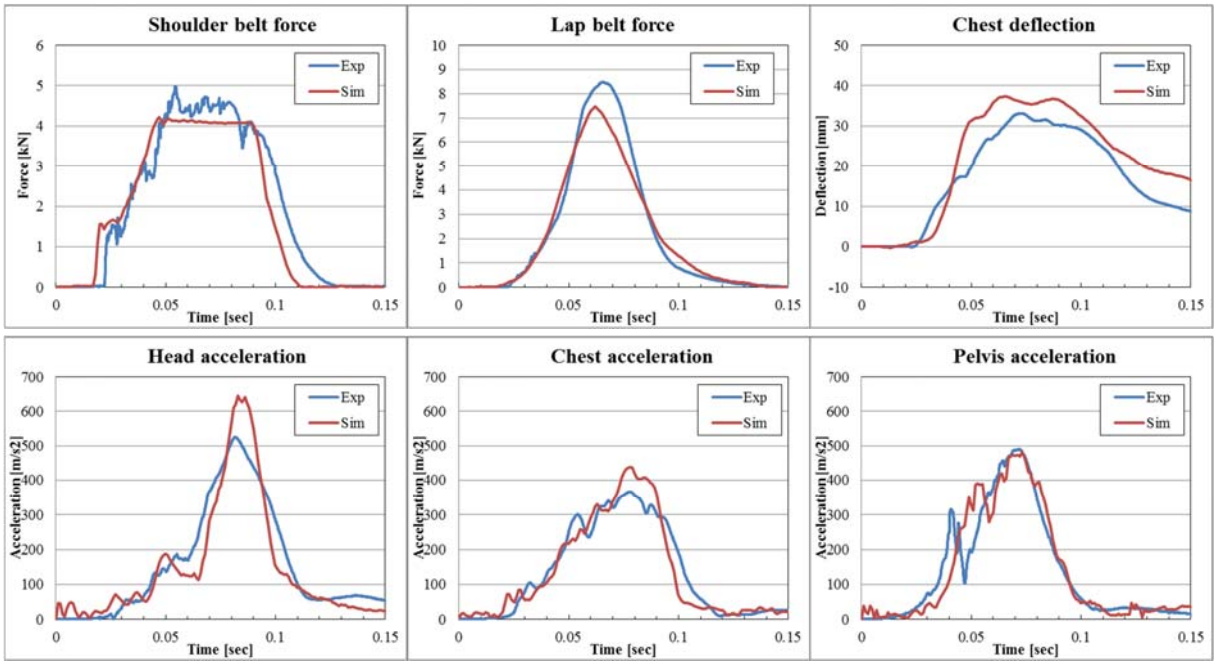

Figure C4. Car interior model evaluation results

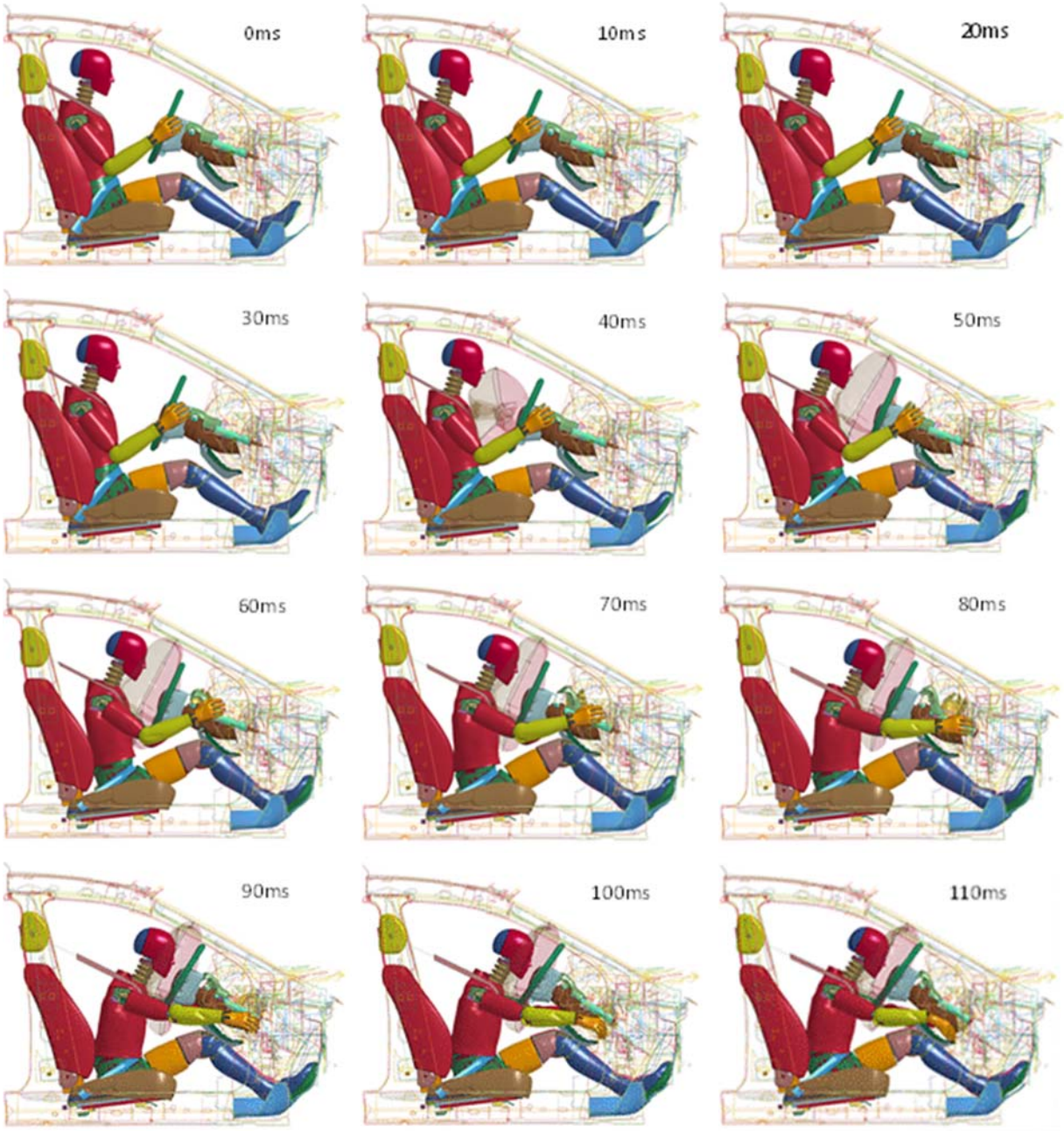

Figure C5. 50th percentile male HIII FE model kinematics with 4 kN belt force limit and Mid airbag

APPENDIX D: Sequences of images from baseline simulation cases (Case 7, Case 19, and Case 31)

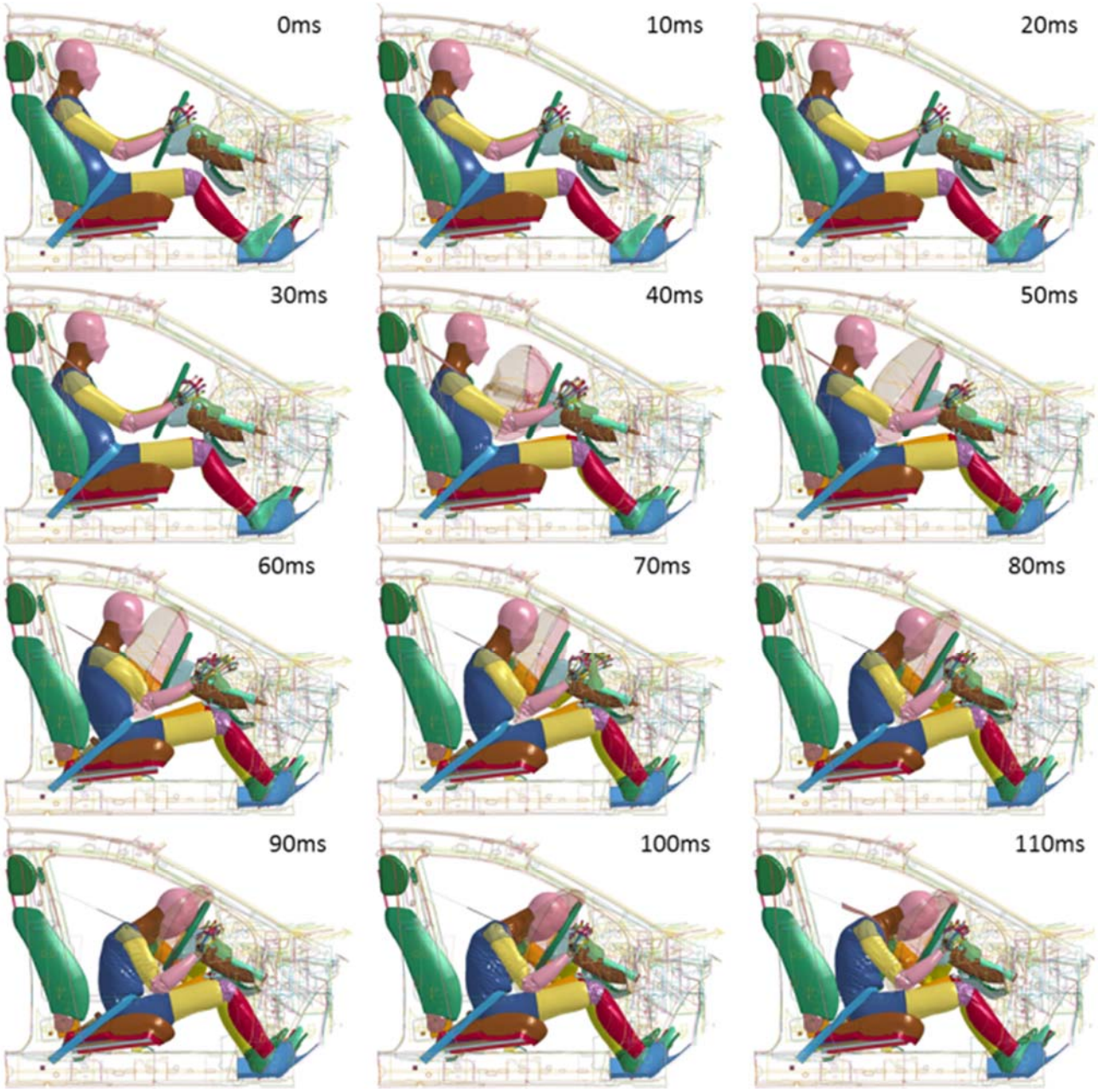

Figure D6. Occupant kinematics for Adult AM50 driver with 4 kN belt force limit and Mid airbag (Case 7)

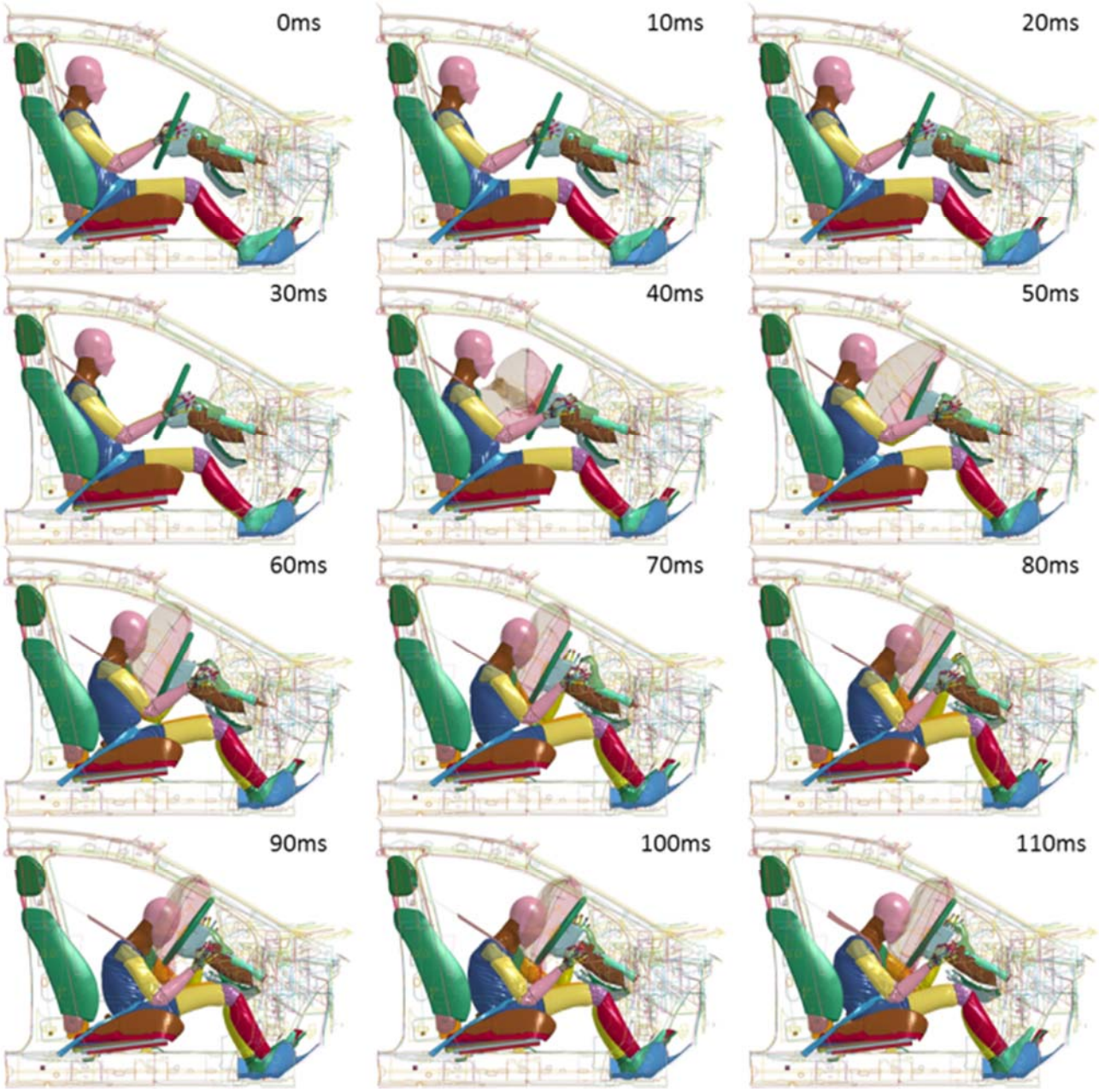

Figure D7. Occupant kinematics for Elderly Small driver with 4 kN belt force limit and Mid airbag (Case 19)

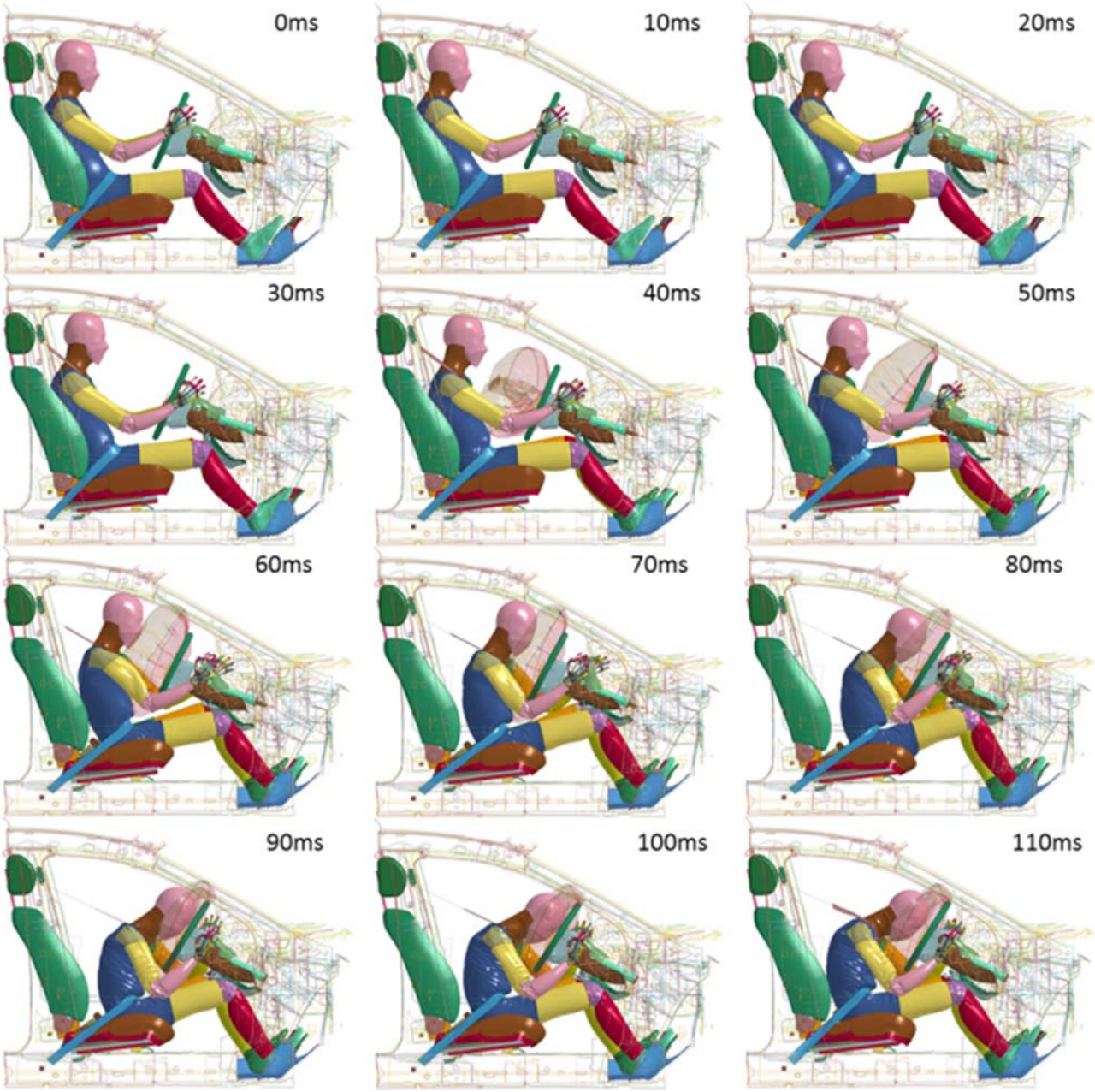

Figure D8. Occupant kinematics for Elderly AM50 driver with 4 kN belt force limit and Mid airbag (Case 31)

APPENDIX E: Seatbelt load, airbag loads, and chest deflections for varying belt force limits

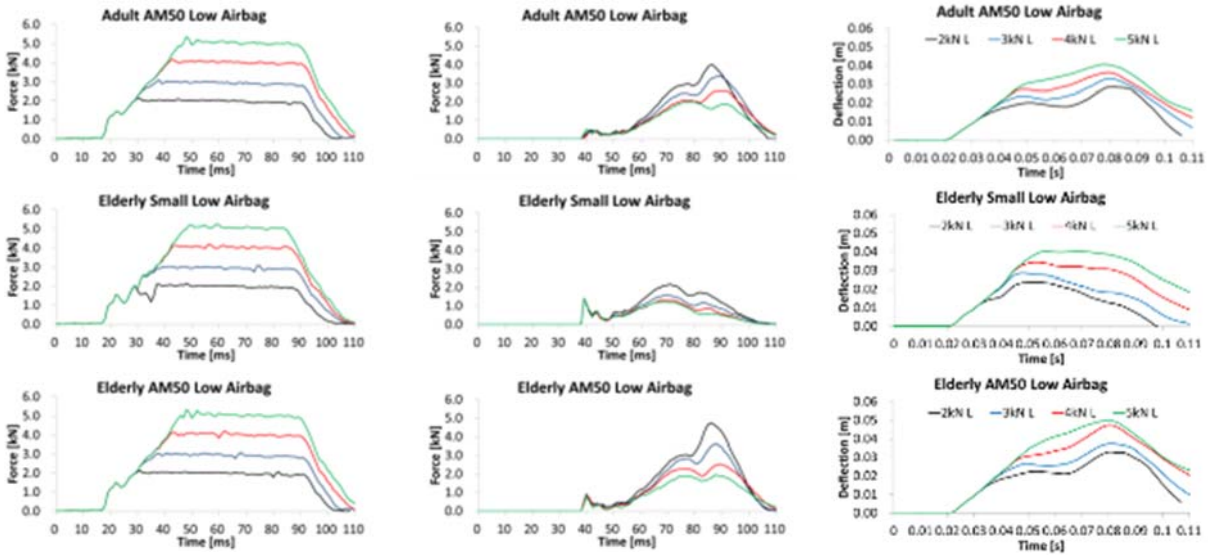

Belt load Airbag load Chest Deflection

Figure E9. Seatbelt load, airbag load, and chest deflection for variable Belt Force limit and constant Low airbag setting

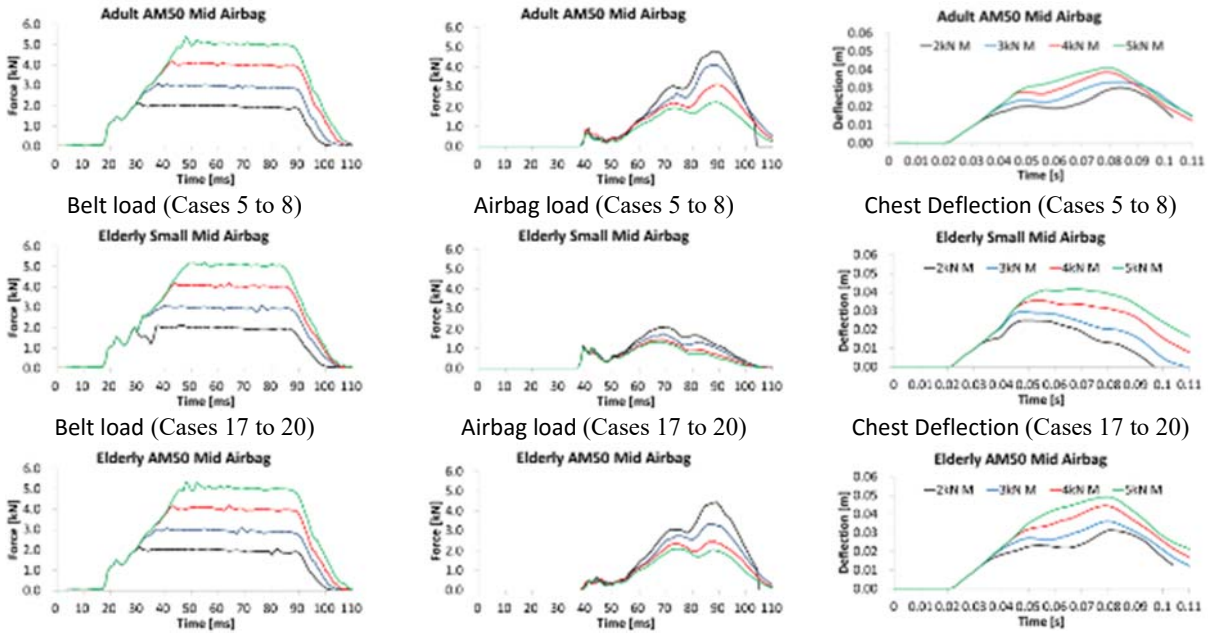

Belt load (Cases 5 to 8) Airbag load (Cases 5 to 8) Chest Deflection (Cases 5 to 8)

Belt load (Cases 17 to 20) Airbag load (Cases 17 to 20) Chest Deflection (Cases 17 to 20)

Belt load (Cases 29 to 32) Airbag load (Cases 29 to 32) Chest Deflection (Cases 29 to 32)

Figure E10. Belt loads (left column), airbag loads (middle column), and chest deflections (right column) for variable belt force limit. Adult AM50 (top row), Elderly Small (middle row) and Elderly AM50 (bottom row) and constant Mid airbag setting

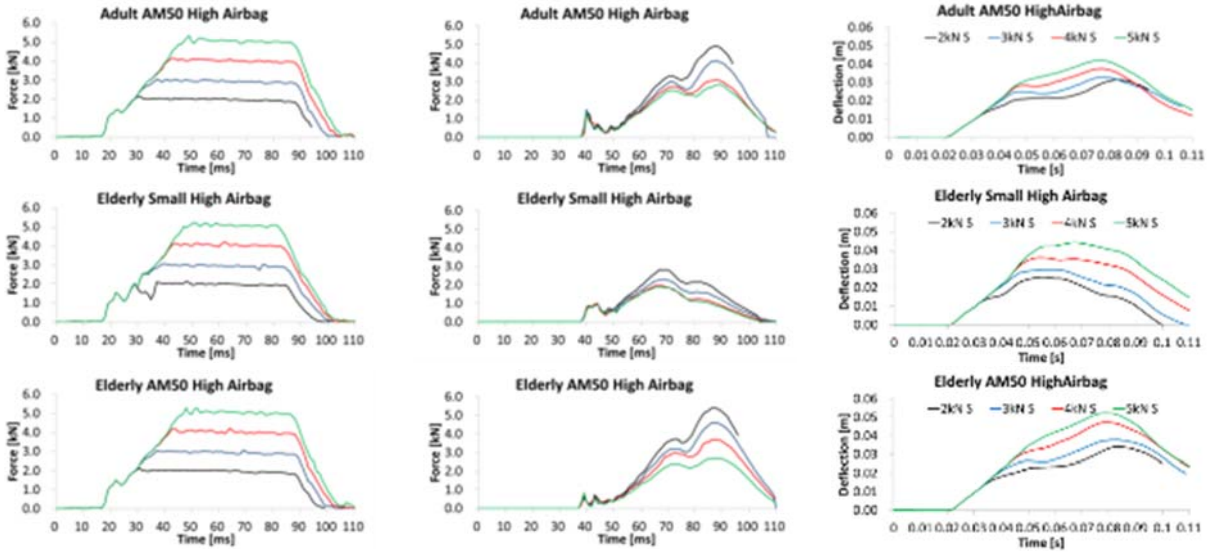

Belt load Airbag load Chest Deflection

Figure E11. Seatbelt load, airbag load, and chest deflection for variable Belt Force limit and constant High airbag setting

APPENDIX F: Seatbelt load, airbag loads, and chest deflections for varying airbag pressure settings

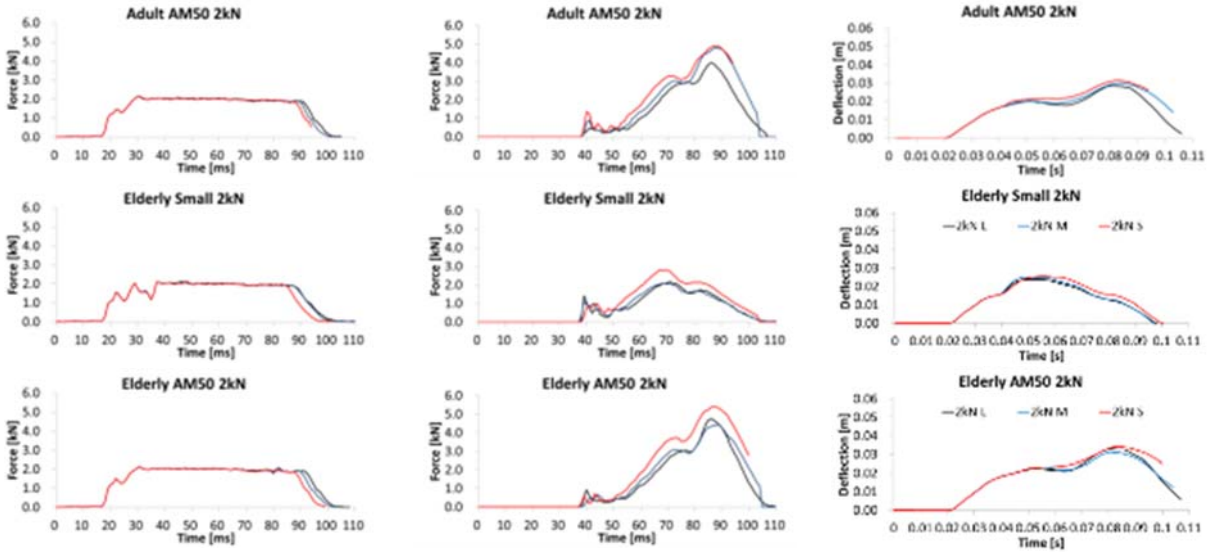

Belt load Airbag load Chest Deflection

Figure F12. Seatbelt load, airbag load, and chest deflection for variable airbag setting and constant 2kN belt force limit

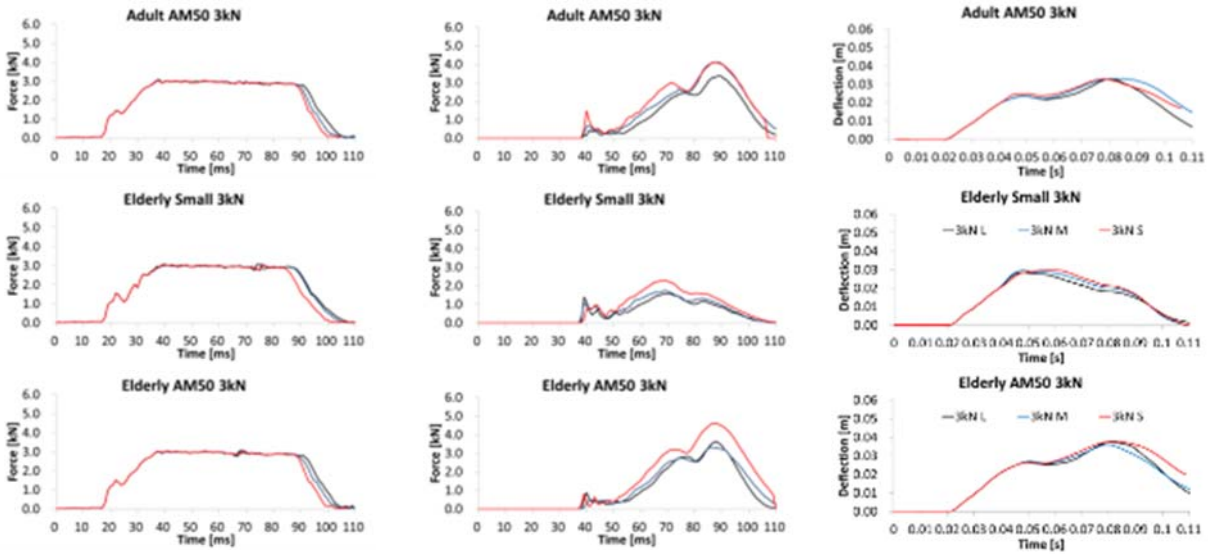

Belt load Airbag load Chest Deflection

Figure F13. Seatbelt load, airbag load, and chest deflection for variable airbag setting and constant 3kN belt force limit

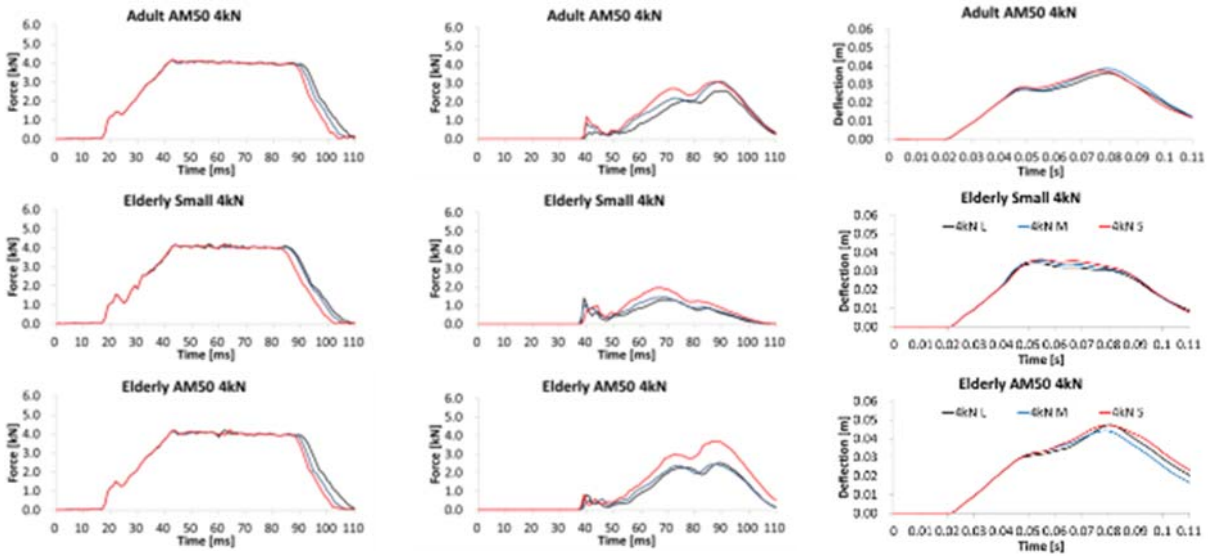

Belt load Airbag load Chest Deflection

Figure F14. Seatbelt load, airbag load, and chest deflection for variable airbag setting and constant 4kN belt force limit

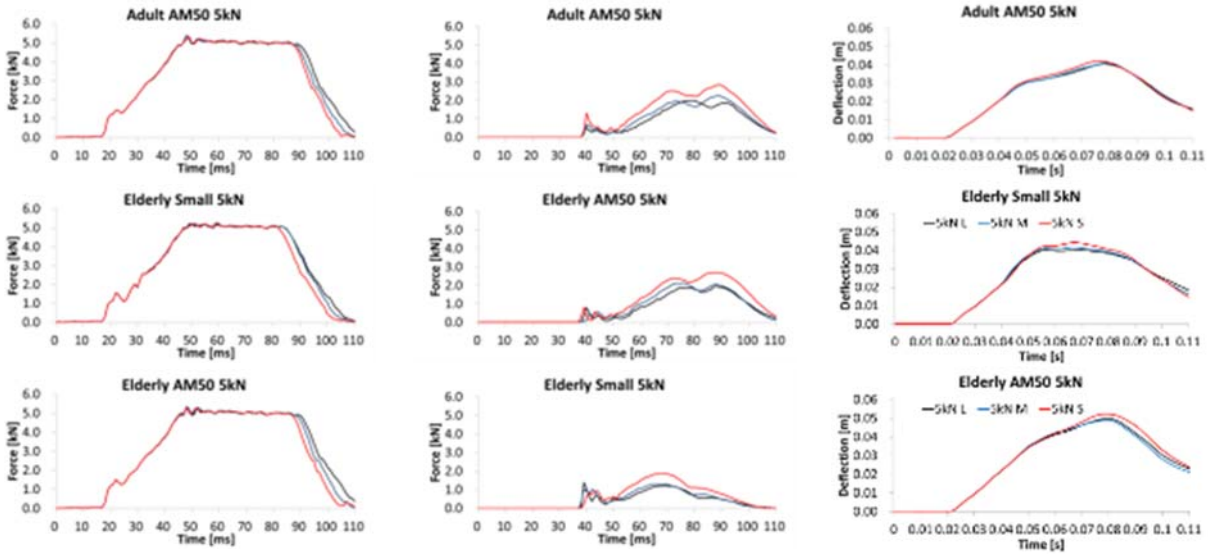

Belt load Airbag load Chest Deflection

Figure F15. Seatbelt load, airbag load, and chest deflection for variable airbag setting and constant 5kN belt force limit

APPENDIX G: Chest deflection and chest excursion for all simulated cases

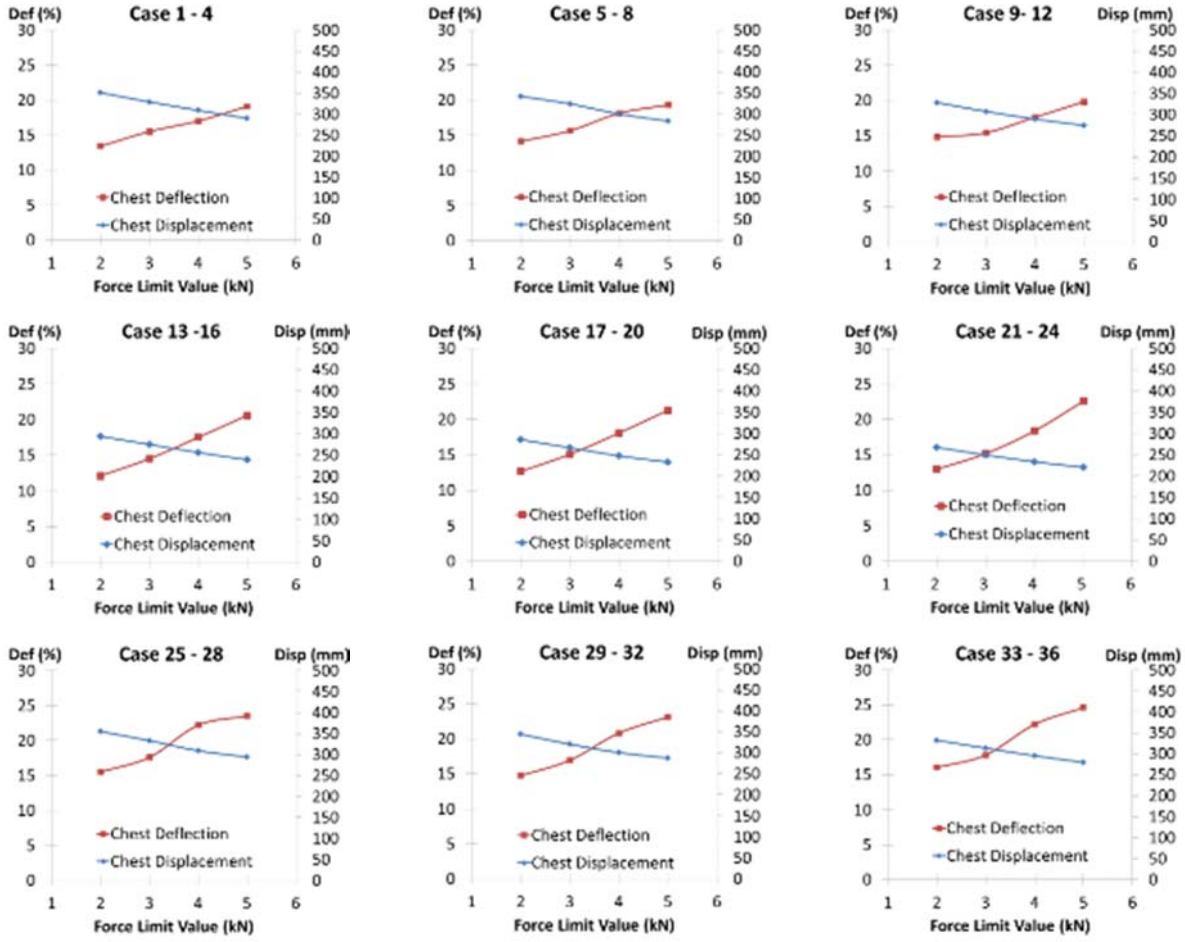

Low airbag Mid airbag High airbag

Figure G16. Chest deflection and chest peak forward excursion as a function of belt force limit for Adult AM50 (Top row), Elderly Small (Mid row) and Elderly AM50 (Bottom row) for Low (Left column), Mid (Mid column) and High (Right column) pressure airbag settings